Role of BMP signaling during early development of the annelid *Capitella teleta*

Nicole B. Webster, Michele Corbet, Abhinav Sur, Néva P. Meyer*

*corresponding author

Clark University

Biology Department

950 Main Street

Worcester, MA 01610-1400

nmeyer@clarku.edu

Abstract

The mechanisms regulating nervous system development are still unknown for a wide variety of taxa. In insects and vertebrates, bone morphogenetic protein (BMP) signaling is known to play a key role in both neural specification and dorsal-ventral (D-V) axis formation, leading to speculation about the conserved evolution of nervous systems. Studies outside insects and vertebrates show a more diverse picture of what, if any role, BMP signaling plays in neural development across Bilateria. This is especially true in the morphologically diverse Spiralia (~Lophotrochozoa). Despite several studies of D-V axis formation and neural induction in spiralians, there is no consensus for how these two processes are related, or whether BMP signaling may have played an ancestral role in either process. Here we incubated larvae of the sedentary annelid *Capitella teleta* in BMP4 protein at various cleavage stages to determine the role of BMP signaling during early development. Adding exogenous BMP protein to early-cleaving *C. teleta* embryos had a striking effect on formation of the brain, eyes, and foregut in a time-dependent manner. However, adding BMP did not block neural specification of the brain or VNC or block formation of the D-V axis. We identified three key time windows of BMP activity, and hypothesize that BMP may cause trans-fate switching of blastomere quadrant identities in at least one time window. 1. Early treatment around 2q caused the loss of the eyes, radialization of the brain, and a reduction of the foregut, which we interpret as a loss of A-, B- and C-quadrant identities with a possible trans-fate switch to a D-quadrant identity. 2. Treatment after 4q induced formation of a third ectopic brain lobe, eye, and foregut lobe, which we interpret as a trans-fate switch of B-quadrant micromeres to a C-quadrant identity. 3. Continuous BMP treatment from early cleavage through mid-larval stages resulted in a modest

expansion of *Ct-chrdl* expression in the dorsal ectoderm and a concomitant loss of the ventral midline (neurotroch ciliary band). Loss of the ventral midline was accompanied by a collapse of the bilaterally-symmetric VNC although the total amount of neural tissue did not appear to be greatly affected. Our results compared to those from other annelids and molluscs suggest that BMP signaling was not ancestrally involved in delimiting neural tissue or establishing the D-V axis in the last common ancestor of annelids. However, the effects of ectopic BMP on quadrant-identity during cleavage stages may represent a very early 'organizing' function in the context of spiralian development. Ultimately, studies on a wider range of spiralian taxa are needed to determine if the ability of BMP signaling to block neural induction and help establish the D-V axis was lost within Annelida or if BMP signaling gained these functions multiple times across Bilateria. Ultimately, these comparisons will give us insight into the evolutionary origins of centralized nervous systems and body plans.

Keywords

Capitella teleta, bone morphogenetic protein, neural specification, Spiralia, Annelida, dorsal-ventral axis

Introduction

Nervous systems are a key feature of most animal taxa, but how evolution produced the wide variety of extant nervous systems is still unknown. Morphologically, nervous systems range from those that are predominantly nerve nets, such as in ctenophores and cnidarians (Hejnol and Rentzsch, 2015; Schmidt-Rhaesa et al., 2015), to those that have a high degree of centralization, e.g. the 'centralized nervous systems' (CNSs) of annelids, insects, and chordates (Arendt et al., 2008; Holland, 2003). The morphological organization of a nervous system can also have functional implications, such as how signals for sensory input and motor output are processed and coordinated. What mechanisms regulate nervous system development, and especially how that differs between taxa, is of particular interest to understand evolution of this complex system.

In insects and vertebrates, the CNS arises from a region of ectoderm that is induced to become neural as part of dorsal-ventral (D-V) axis specification, although the neuroectoderm is dorsal in vertebrates and ventral in insects. D-V axis formation relies in part on a gradient of Bone Morphogenetic Protein (BMP) signaling that also inhibits neural induction (De Robertis and Kuroda, 2004; Holley et al., 1995; Wilson and Edlund, 2001). The similarities between vertebrate and insect neural induction, where BMP signaling plays an anti-neural role, have

prompted speculation that the last common ancestor of Bilateria had a CNS that was localized along a D-V axis (Arendt and Nubler-Jung 1999; Denes et al. 2007; De Robertis 2008). However, comparison of data from a wider range of taxa from deuterostomes and ecdysozoans shows less support for this hypothesis (see Discussion).

Examining new systems can lead to a new perspective into neural development and evolution. Spiralia (≈Lophotrochozoa) includes taxa with widely divergent body plans such as annelids, molluscs, brachiopods, rotifers, and platyhelminths (Kocot et al., 2016). These diverse morphologies include a great variety of nervous systems, from the highly intelligent brains of cephalopods (Shigeno et al., 2018) to the rope-ladder-like ventral nerve cords in a subset of annelids (Helm et al., 2018) to a single suboesophageal ganglion in inarticulate brachiopods (Nielsen, 2005). Such diversity leads to opportunities for comparative studies to understand the evolutionary origins of CNSs. Spiralians have an added benefit for studying the evolution of body plans, including the CNS. Developmentally many taxa share an ancestral stereotyped cleavage program called spiral cleavage (Giribet et al., 2009) where each cell (blastomere) acquires distinct fates during embryogenesis that contributes to a specific set of tissues.

Annelids have a CNS comprising an anterior brain and a VNC (Muller, 2006), but it is unclear if BMP signaling is involved in early D-V axis formation and/or neural specification of the CNS. Despite several studies of D-V axis formation and neural induction in spiralians, there is no consensus for how these two processes are related, or whether BMP signaling may have played an ancestral role in either process. In the mollusc *Tritia (=Ilyanassa) obsoleta*, knocking down BMP signaling during early cleavage stages resulted in a similar phenotype to removing the organizer signal (i.e. removing the polar lobe), including a disrupted D-V axis. In contrast, adding BMP4 protein partially rescued the removal of the polar lobe (Lambert et al., 2016). While BMP signaling appears to be part of the organizer in this animal, exogenous BMP protein caused ectopic eye and likely brain formation rather than a loss of neural tissue as seen in vertebrates and insects, and no effect on trunk neural tissue was reported (Lambert et al., 2016). These data suggest that BMPs may actually induce neural tissue in *T. obsoleta* rather than block it as in vertebrates and insects. In *Crepidula fornicata,* another mollusc, BMP protein induced a pinching off of part of the episphere, while the trunk stayed relatively normal including a D-V axis and neural tissue formation (Lyons et al., 2020).

Here we further explore the role of BMP signaling during neural development in the annelid *C. teleta*. By exposing embryos at different timepoints to exogenous BMP protein, we show the importance of timing in the role BMP plays for neural development, as well as key differences

between the effects on the trunk and episphere. BMP treatment at early cleavage stages, when the organizer is likely signaling, resulted in animals with an intact D-V axis and a VNC, but there was a loss of eyes, brain lobes and foregut tissue. At later cleavage stages, BMP exposure resulted in the formation of a third ectopic eye, brain lobe, and foregut lobe. Only with continuous BMP exposure did a clear trunk phenotype appear where ventral midline structures were lost. The loss of the ventral midline also resulted in a collapse of the VNC where the VNC neurites were localized to the ventral midline; however, most of the neural tissue in the VNC was still present, and the overall D-V axis did not appear to be greatly affected.

Material and Methods

Animal care and embryo collection

Adults of *Capitella teleta* Blake et al. (2009) were cultured in glass finger bowls with 32–34 ppt artificial sea water (ASW) at 19 °C and fed with sieved mud (Grassle and Grassle, 1976; Meyer et al., 2015; Seaver et al., 2005). Embryos of the correct stage were collected from females with broods produced from mating dishes by combining males and females after keeping them separate for 3–5 days. Embryos were collected 12-16 hours (h) after assembling the mating dish or by exposing the dish to light for 6+ h, then combining them 5 h prior to collecting zygotes (Lanza and Seaver, 2020a). Embryos and larvae, except where otherwise noted, were raised in ASW with 50 ug/mL penicillin and 60 ug/mL streptomycin (ASW+PS) in the dark at room temperature (RT, ~21 °C). ASW+PS was changed twice daily. Prior to fixation, all larvae were relaxed in 1:1 ASW:0.37 M $MgCl_2$ for 5–10 min.

Embryos were staged by the birth of all four micromeres for a specific quartet except for the 4th quartet, where only birth of 4d was monitored due to the difficulty in seeing 4a–4c being born. Thus 1st-quartet (1q), 2nd-quartet (2q), and 3rd-quartet (3q) embryos had micromeres 1a–1d, 2a–2d, and 3a–3d, respectively. 4th-quartet (4q) animals were incubated in BMP or mock solution (see below) starting ~40 min after the appearance of micromere 4d.

Incubation in BMP protein

Embryos of the desired stage were isolated from a single brood and washed several times in ASW+PS. Healthy embryos—without any signs of lysis—were separated into 0.2% gelatin-coated four-well culture dishes (Nunc, BioExpress cat. 144444) in 400 µL ASW+PS. For exogenous BMP treatment, animals were incubated in 250 ng/mL recombinant zebrafish BMP4 protein (R&D Systems, cat. 1128-BM-010) in 0.1% bovine serum albumin (BSA) and 0.04 mM HCl in

ASW+PS. BMP4 protein was stored as 5 or 10 uL aliquots at a stock concentration of 20 µg/mL in 4 mM HCl + 0.1% BSA at -80 ˚C. The two control groups included: 1) 400 µL ASW+PS (control), and 2) 5 µL 0.1% BSA in 4 mM HCl (mock) in 400 µL of ASW+PS. Animals were raised at RT until stage 6 (Seaver et al., 2005), and solutions were changed every 12 h for continuous (cont) BMP experiments. After BMP incubation, animals were washed several times with ASW+PS to remove residual BMP or mock solutions (Fig. 1).

Isolation of *C. teleta* BMP pathway gene homologs

Total RNA was extracted from mixed stage 1–9 embryos and larvae using the RNA Trizol extraction protocol (Molecular Research Center, Inc.) or the RNeasy Mini Kit (Qiagen). Reverse transcription reactions were conducted using the SMARTer RACE kit (Clontech) or High capacity cDNA Reverse Transcription kit (Applied Biosciences). *Capitella teleta* has one *chordin-like* (*Ct-chrdl*) and one *bmp5-8* homolog (Kenny et al., 2014). A 940 bp fragment of *Ct-chrdl* (JGI PID224618) coding sequence was amplified by PCR using gene-specific primers: *Ct-chrdl*: 5'-ACACGAATGGAGCAGTAACTTG and 5'- AGCGCTCTGTCAGTAATTTTCA and nested primers 5'-AGAAACGCACAAGAGCCAAC and 5'-AGAAACGCACAAGAGCCAAC. A 1445 bp fragment of *Ct-bmp5-8* (JGI PID172350) was used to make a probe with primers: 5'-ATGCTCGCTGCTTTCGCCG and 5'-CAGCTTCGTTGGCAGCAAT. PCR products were TA-cloned into the pGEM-T Easy vector (Promega) or PCRII vector (Invitrogen) and sequenced. These gene fragments were used as a template to generate DIG-labeled anti-sense RNA probes using MegaScript SP6 or T7 transcription kit (ThermoFisher Scientific) for whole mount in situ hybridization (WMISH). The probe *Ct-elav1* has been previously described (Meyer and Seaver, 2009).

Whole Mount *In situ* Hybridization

WMISH was conducted as described previously (Seaver et al. 2001). Briefly, all WMISH fixations were done in 4% paraformaldehyde (PFA, stock 32% PFA ampules from Electron Microscopy Sciences, cat. 15714) in ASW for 6 h–overnight at 4°C. After fixation, animals were serially dehydrated in methanol and stored at -20 °C. Animals were hybridized for a minimum of 72 hours at 65 °C with 1 ng/µl of each probe. DIG-labeled RNA probes were generated using the MegaScript SP6 or T7 transcription kit (ThermoFisher Scientific). Spatiotemporal RNA localization was observed using an NBT/BCIP color reaction. After WMISH, animals were labeled with Hoechst 33342, cleared in 80% glycerol in PBS, and mounted on slides for DIC and fluorescent imaging.

Staining and antibody labeling

Immunolabeling was carried out as in Meyer et al. (2015). Briefly, animals were fixed with 4% PFA in ASW, rinsed with PBS and PBT (PBS + 0.1% Triton-X 100), blocked in 5 or 10% goat serum and incubated in primary antibody overnight at 4 °C. Secondary antibody labeling was also performed overnight at 4 °C, then animals were cleared and mounted in 80% glycerol in PBS. All washes and exchanges were done in RainX-coated glass spot dishes. Primary antibodies used were as follows: 1:800 rabbit anti-serotonin (5HT; Sigma-Aldrich, cat. S5545), 1:10 anti-Pax (clone DP311, (Davis et al., 2005), 1:800 rabbit anti-FMRFamide (Immunostar, cat. 20091), 1:20 mouse anti-Futsch (clone 22C10, Developmental Studies Hybridoma Bank), 1:800 mouse anti-acetylated tubulin (clone 6-11B-1, Sigma, cat. T6793), 1:50 anti-Synapsin (clone 3C11, Developmental Studies Hybridoma Bank). Secondary antibodies used were as follows: 1:2000 goat anti-mouse F(ab')2 Alexa488 (Sigma-Aldrich, cat. F8521) and 1:1000 sheep anti-rabbit F(ab')2 Cy3 (Sigma-Aldrich, cat. C2306) in block. F-actin and DNA staining were performed by incubating the embryos in 1:100 BODIPY FL-Phallacidin (Life Technologies, cat. B607; stock concentration 200 Units/mL in methanol), 0.1 µg/mL Hoechst 33342 (Sigma-Aldrich, cat. B2261), and/or 1:1000 ToPRO3-iodide in PBS according to Meyer et al. (2015, 2010).

DiI labeling

Pressure injection of the lipophilic DiI (1,1'-dioctadecyl-3,3,3'3'-tetramethylindocarbocyanine perchlorate, Invitrogen) has been described previously (Meyer et al., 2010; Sur et al., 2020). DiI was injected into the 1a or 1b micromeres, and animals were monitored for normal cell division of all micromeres after injection. BMP4 protein in ASW+PS was added after birth of the 4d micromere and embryos were incubated for 12 h at RT and then for an additional 3.5 days in ASW+PS at RT. Animals were then fixed and labeled with Hoechst and Phallacidin in PBS as previously described (Meyer et al. 2010).

Western blot

Larvae were collected in 1.5 mL microcentrifuge tubes, and then briefly centrifuged in a minifuge to concentrate animals at the bottom of the tube. As much ASW as possible was removed, and the larvae were flash frozen in liquid nitrogen and stored at -80°C until use. Tissue was lysed just prior to use in a lysis buffer (50mM Tris (pH=8.0), 150mM NaCl, 1% Triton X-100) with a mortar and pestle (Electron Microscopy Sciences, 64788) and a LabGen 7B homogenizer (ColePalmer, EW-04727-09). Tissue was then denatured at 100 °C for 5 min after adding 1:1 SDS-PAGE (0.1M Tris-HCl (pH 6.8), 4% w/v SDS, 20% v/v Glycerol, 0.025% BPB (bromophenol blue) and 0.68 µL β-Mercaptoethanol. The resultant tissue lysate was run on a

precast SDS-PAGE gel (4-20% MP TGX Stain-Free Gel, Bio-Rad 4568093), with a Precision Plus Protein WesternC Stds ladder (Bio-Rad 1610376). Total protein was visualized with a stain-free viewer (Bio-Rad EZ imager) to confirm an even amount of protein in each lane. The protein was and transferred to a Polyvinylidene difluoride (PVDF) membrane (Bio-Rad, 1704274) with a turbo transfer system (Bio-Rad) for 30 mins. Blots were blocked with 5% BSA in TBST (20mM Tris (pH=7.5), 150mM NaCl, 0.1% Tween-20), incubated with a 1:1000 dilution of anti-phosphorylated-SMAD1/5/8 (clone 41D10, Cell Signaling Technologies) or anti-phosphorylated-SMAD2/3 (clone D27F4, Cell Signaling Technologies) and hybridized with a 1:2000 dilution of horseradish peroxidase-linked anti-rabbit IgG secondary antibody (A24537 Life Technologies), and Streptactin-HRP to visualize the ladder. The protein was visualized with Clarity ECL (Bio-Rad, 1705060) on a LAS-4000 (GE) imager.

Microscopy

Images were taken using DIC optics on a Zeiss M2 microscope with an 18.0 megapixel EOS Rebel T2i digital camera (WMISH, Canon) or an AxioCam MRm rev.3 camera (Zeiss), and Zen Blue software (Zeiss) was used to capture the images. Animals for confocal laser scanning microscopy (CLSM) were cleared and mounted in SlowFade® Gold (Life Technologies, cat. S36936) and imaged using a TCS SP5-X (Leica). Z-stacked images were merged with Helicon focus 7 (Helicon); Zen Blue (Zeiss) was used to merge fluorescent images, WMISH images were edited for contrast and brightness using Adobe Photoshop CC (Adobe), and the figure panels were assembled with Adobe Illustrator CC (Adobe).

Phenotypic scoring

Eye pigment

Larvae were scored for the presence/absence and location of the orange larval eye pigment cell shortly following fixation as the eye pigment fades rapidly, within a week after fixation. They were scored in PBS using a Zeiss Stereo Lumar V.12 stereomicroscope. Three-eyed animals were scored in two categories: stacked, where the third eye was in close proximity to one of the endogenous eyes, and centered, where the third eye was along the ventral midline approximately equidistant to either of the endogenous eyes.

Brain 5HT localization

Anterior z-stacked images were scored for the locations of $5HT^+$ neuronal cell bodies relative to the position of the prototroch and foregut. In Fiji (Schindelin et al., 2012), the episphere was

divided into 8 sections (octets: dorsal, left, ventral, right, and the 4 intervening regions), and each 5HT$^+$ soma was scored for position within the octets.

Measurements

All measurements were made using Fiji. Animal length was measured from prototroch to telotroch to control for episphere shape variation, and widths were measured at segment 4 which is approximately midway along the animal trunk at stage 6.

Foregut measurements were made using the Hoechst nuclear stain from a ventral view, and measurements were taken at the same focal plane as the ventral mesodermal bands in order to maximize foregut area. Total foregut area was measured including the interior space. Foregut shape was also scored as normal, small, or three-lobed.

The total width of *Ct-chrdl* expression was measured from dorsal images at segment 4. In animals expressing *Ct-bmp5-8*, the width of the dorsal midline tissue between the two bands of *Ct-bmp5-8* expression was measured from a dorsal view but was highly variable even within a single animal. The total width of *Ct-elav1* expression in the VNC was measured from left to right from ventral images at segment 4. To calculate the amount of neural tissue, the width of the ventral midline tissue not expressing *Ct-elav1* was also measured, and this width was subtracted from the total *Ct-elav1* width.

Statistics and graphing

All statistics were performed in R/RStudio 1.2.5 (R Core team, 2014; RStudio Team, 2012), and all graphs were created using the ggplot2 package (H. Wickham, 2009) and polished with Adobe Illustrator CC (Adobe). Model testing was used in each case to determine the appropriate covariables to analyze in each ANOVA; the R package rcompanion (Mangiafico, S.S., 2015) was used, and the model with the lowest AIC was chosen.

Mean circular orientation of 5HT$^+$ neurons in the episphere was analyzed using a model-based maximum likelihood approach to test multiple possible orientations (Fitak and Johnsen, 2017). The best model to fit the data was chosen using a likelihood ratio test and default settings in the CircMLE package.

Results

BMP treatment in *C. teleta* increases pSMAD1/5/8 levels

Incubating embryos and larvae in recombinant BMP protein is an effective way to test BMP function during different developmental time windows. To confirm the ability of recombinant zebrafish BMP4 protein to activate the BMP pathway in *Capitella teleta*, we assayed levels of phosphorylated Ct-SMAD1/5/8 (pSMAD1/5/8) in BMP-treated animals by western blot analysis using an antibody against the C-terminus of mammalian pSMAD1/5 (41D10, Cell Signaling Technologies). The transcription factor SMAD1/5/8 is phosphorylated by BMP receptor 1 (BMPR1) once bound by a BMP ligand. pSMAD1/5/8 then binds SMAD4 and is transported into the nucleus where it affects gene transcription (Gámez et al., 2013). High pSMAD levels are an indicator of an active BMP signaling pathway. BMP treatment of 2q cleavage-stage embryos (n=40/treatment) for 10 min, 1 h, 3 h, and 6 h resulted in an increase in three separate bands (~27, 33, and 65 kDa) on the western blot relative to mock treatment of 2q embryos for 6 h (Fig. 2). The same pattern of pSMAD bands and the same pattern of up-regulation was observed on western blots after treating *C. teleta* cleavage-stage embryos with BMP4 protein for various amounts of time (data not shown).

Capitella teleta has one SMAD1/5/8 homolog (Kenny et al., 2014) that contains a 5' truncation in the genome sequence (Lanza and Seaver, 2020b) and the expressed mRNA. We confirmed that this was not present in related animals, including other annelids and molluscs such as *Helobdella robusta, Crassostrea gigas,* and *Crepidula fornicata*. *Ct-smad1/5/8* is approximately 920 bp (vs 1395 bp in *H. robusta*) and lacks the MH1 domain, which is involved in DNA binding (Heldin et al., 1997), as well as the nuclear localization signal and one of two nuclear export signals (Xiao et al., 2003). This should produce a protein that is 279 aa or ~31 kDa. Full-length SMAD1/5/8 homologs in other animals, which do not contain this truncation, are predicted to be ~51 kDa (Fig. 3). We interpret the lower, ~27, 33 kDa bands on our westerns as phosphorylated Ct-SMAD1/5/8. The upper band may represent the related pSMAD2/3, which is predicted to be ~50 kDa in *C. teleta* (Kenny et al., 2014). However, we think this unlikely due to the lack of D-V phenotypes in the trunk after treatment with recombinant BMP protein (see Discussion). Another possibility is that Ct-SMAD1/5/8 has an alternative start site or that there is a second SMAD1/5/8 homolog in *C. teleta* that has yet to be identified in the genome. Taken together, we interpret the increase in the bands on the pSMAD1/5/8 western as evidence that exogenous addition of recombinant BMP protein is able to activate the BMP signaling pathway in *C. teleta*.

BMP treatment in *C. teleta* does not affect overall A-P and D-V axis formation

To assess the effect of exogenous BMP at different times during embryogenesis, *Capitella teleta* embryos were incubated in exogenous BMP4 protein for 12-hours (pulse) or continuously (cont) starting as early as birth of the first-quartet of micromeres (referred to as "1q"), i.e. 8-cell embryos, through mid-larval stages, usually stage 6 (Fig. 1). Additional starting times included: once the second-quartet micromeres were born (2q), once the 3rd-quartet micromeres were born (3q), once 4d was born (4q), and at various timepoints after birth of 4d until the beginning of gastrulation (Fig. 1). Gross morphology was assayed by DIC microscopy, and, in general, features along both the dorsal-ventral (D-V) and anterior-posterior (A-P) axes were correctly localized relative to one another in stage 6 (Fig. 4) and stage 7 larvae. For the D-V axis, features examined included the foregut, chaetae, VNC, and neurotroch, and features examined along the A-P axis included the brain, prototroch, foregut, and telotroch. Overall, our data suggest that neither the D-V nor A-P axes were greatly affected by BMP treatments at any of the time windows examined.

To further assess overall development following BMP treatment, number of trunk segments was counted using a nuclear stain (Hoechst). The number of trunk segments in BMP-treated animals was significantly reduced compared to controls even when controlling for animal length (2-way ANOVA treatment|animal length, $F_{treatment} = 33$, df = 3, $p < 0.001$). There were significantly fewer segments produced with earlier BMP treatment (1q vs 4q), but not with a longer time of BMP treatment (1q pulse vs. 1q cont) (Tukey HSD, $p < 0.01$). Mock animals (experimental control containing only solvent and no BMP4 protein) had a mean of 12 ± 1 SD segments whereas 1q pulse and 1q cont animals had 9 ± 1 SD segments each and 4q pulse had 11 ± 2 SD segments. Adding BMP4 protein reduced the number of segments produced in a timing-dependent manner, which could be indicative of a slight developmental delay. This is further supported by a slight delay noticed for onset of swimming behavior in the BMP-treated animals (not scored).

Expression of the dorsal ectodermal markers *chordin-like* and *bmp5-8* is spatially shifted after BMP treatment

Although the formation of the D-V axis did not appear to be greatly affected in *C. teleta* larvae treated with BMP protein, we examined the expression of markers in the dorsal ectoderm since BMP signaling has been reported to pattern D-V fates within the ectoderm in two other annelids (Denes et al., 2007; Kuo et al., 2012). Chordin-like homologs in other animals antagonize BMP signaling (Branam et al., 2010), and *Ct-chordin-like* (*Ct-chrdl*) is dorsally expressed in the ectoderm starting at stage 5 (Fig. 5A), as is *Ct-bmp5-8* (Webster et al., in prep). *Ct-chrdl*

expression was significantly wider (laterally) in BMP-treated animals when compared to mock animals, even when animal width and length were considered (ANOVA, $F_{treatment} = 16.7$, df = 3, $p < 0.001$, Fig. 5B, compare with 5A). All three treatments examined, 1q cont, 3q cont, and 3q pulse animals, had a wider domain of dorsal *Ct-chrdl* expression than mock animals (Tukey HSD, $p < 0.07$). There was no observed difference in the anterior-posterior extent of *Ct-chrdl* (Fig. 5A, B).

Ct-bmp5-8 is expressed as two stripes in the dorsal-lateral ectoderm starting at stage 5, on either side of the dorsal *Ct-chrdl* stripe. In agreement with the increased domain of *Ct-chdl* expression, the dorsal boundaries of the *Ct-bmp5-8* stripes were shifted more ventrally (i.e. the width between left at right bands of expression was greater) with a 1q or 3q pulse of BMP (data not shown).

BMP treatment does not block brain or VNC formation during early cleavage stages

To look at the effect of BMP treatment on neural tissue, we first examined formation of the brain and VNC using the marker *Ct-elav1* (Fig. 6), which is expressed throughout the nervous system in post-mitotic neurons (Meyer and Seaver, 2009; Sur et al., 2020, 2017). In the episphere after BMP treatment, *Ct-elav1* was expressed in the brain, but the tissue organization was grossly affected with varying location and number of brain lobes (Fig. 6E, I, M). Furthermore, the episphere of BMP-treated animals appeared smaller, with the *Ct-elav1*$^+$ tissue comprising a larger proportion (data not shown). 1q pulse and 1q cont animals generally showed a disorganized pattern of *Ct-elav1* (Fig. 6E, M), while 4q pulse animals generally had three brain lobes based on nuclear staining, all of which expressed *Ct-elav1* (Fig. 6I; further discussed below).

Overall, *Ct-elav1* expression in the VNC of animals treated with a pulse of BMP starting at 1q or 4q was similar to that in wild-type and mock animals, with bilaterally-symmetric expression in the ganglia on either side of the ventral midline (compare Fig. 6F–H, J–L with Fig. 6B–D,). However, in animals treated continuously with BMP from 1q to larval stage 6, *Ct-elav1* was expressed in the ganglia of the VNC, but the ventral midline gap was missing between the left and right hemiganglia in each segment (Fig. 6N, P). While BMP treatment did not appear to block formation of the VNC, and the neural tissue was still ventrally-positioned in the trunk (e.g. Fig. 6G, K, O), we also quantified whether BMP treatment affected the amount of neural tissue within a segment. This was done by measuring segment 4—where the most severe collapse was evident in continuously-treated animals. The total width from left to right of the *Ct-elav1*

expression domain was measured, and the midline gap was excluded to approximate the total amount of neural tissue in that segment. BMP treatment in 1q and 4q pulse animals did not significantly affect the total width of *Ct-elav1* expression minus the midline gap relative to mock-treated animals; Mock (n = 37), 67.0 ± 4.6 µm (SD); 1q pulse (n = 36), 60.0 ± 6.7 µm (SD); 4q pulse (n = 36), 61.7 ± 6.1 µm (SD)). In contrast, cont 1q BMP treatment had a significant effect on the width of tissue expressing *Ct-elav1* (ANOVA, $F_{treatment} = 78$, df = 3, $p < 0.001$; Tukey's HSD, $p < 0.001$, Fig. 6), where 1q cont animals had a significantly narrower expression domain in segment 4 (Mean width: 1q cont (n = 45), 50.3 ± 13.6 µm (SD); Fig. 6P). This pattern also held true for the width of *Ct-elav1* expression, *including* the midline gap (data not shown), and was not affected by animals size (model testing; prototroch–telotroch length). Taken together, these data suggest that pulses of BMP at 1q and 4q do not change the amount of neural tissue in the VNC, at least in segment 4, while continuous BMP treatment at 1q does reduce the amount of neural tissue in segment 4 (~25% reduction) even when the loss of the non-neural midline tissue is taken into account.

We also found that BMP treatment had a significant effect on the A-P length of tissue expressing *Ct-elav1* even when the prototroch-telotroch length was accounted for (2-way ANOVA treatment| prototroch-telotroch length, $F_{treatment} = 58.7$, df = 3, $p < 0.001$). All treatments produced a significantly shorter *Ct-elav1* expression region (i.e. VNC) than in mock animals (Figure 6); however, BMP treatment was also found to reduce the total number of segments (see "BMP treatment in *C. teleta* does not affect overall D-V axis formation" above).

BMP treatment during late cleavage stages resulted in a loss of ventral midline structures and collapse of the VNC

To further examine the architecture of the VNC after BMP treatment, we examined nuclei, neurites (anti-acetylated Tubulin staining), and serotonergic neurons in late stage 6/early stage 7 larvae. BMP did not have a strong effect on formation of the VNC in 1q pulse, 4q pulse, or stage 3 cont treatments (Fig. 7). The ganglia, longitudinal connectives, commissures, and $5HT^+$ neurons in the VNC and the peripheral nerves in each segment were clearly visible (Fig. 7). There appeared to be a slight developmental delay in the number of $5HT^+$ longitudinal connectives in the 1q and 4q pulse animals (compare 7B, C with Fig. 7A), and the longitudinal connectives appeared disorganized in larvae treated from stage 3 to late stage 6 (Fig. 7D).

Since continuous BMP treatment starting at 1q resulted in expression of *Ct-elav1* across the ventral midline at stage 6, we further examined formation of the neurotroch (ventral midline structure) and the architecture of the VNC using Hoechst (nuclei) and cross-reactive antibodies

against acetylated-Tubulin (cilia and neurites), serotonin, FMRF, Synapsin, and Pax (Figs. 8 and 9). Animals were treated continuously with BMP protein starting at 1q, 2q, 3q, 4q, 4q+6h, 4q+12h, 4q+18h, 4q+22h (just prior to the onset of gastrulation), and stage 3 (onset of gastrulation) until stage 6. The severity of VNC collapse varied from complete collapse along the anterior-posterior extent of the trunk to a mild collapse of the VNC in a few segments. In the most severe cases, all five main connectives of the VNC (acetylated-Tubulin, Synapsin), including the three 5HT$^+$ connectives and the two FMRF$^+$ connectives, formed a single track along the midline (Fig. 8B, E; Fig. 9D, E). Furthermore, the left and right hemiganglia appeared continuous across the midline in all segments (Fig. 8H), the cilia of the neurotroch (ventral midline ciliary band) were not detectable (Fig. 8N), and subsets of Pax$^+$ neural cells that are normally bilaterally-symmetric in each segment appeared closer to the ventral midline (Fig. 9F). Interestingly, while most of the cilia of the neurotroch were lost, the cilia around the mouth were present (see Fig. 8N, O), even in animals with the most severe midline loss. It is worth noting that the ciliary cells around the mouth arise from a different blastomere lineage than the rest of the ciliary cells in the neurotroch (3c and 3d versus 2d^2 and 2d^{12}, respectively) (Meyer et al., 2010; Meyer and Seaver, 2010). We also saw a range of intermediate phenotypes, including BMP-treated animals with no midline abnormality (data not shown) and animals with a 'mild' phenotype consisting of VNC collapse, hemiganglia intercalation, and patchy reduction of neurotroch cilia in a few segments (Fig. 8C, F, I, L, O). We did not observe VNC collapse or loss of the neurotroch in mock-treated animals or in animals treated with a 12 h pulse of BMP protein starting at 1q, 2q, 3q or 4q.

To determine the timing critical to cause VNC collapse, we quantified the proportion of segments with collapsed hemiganglia from cont BMP treatment starting at different times. The degree of VNC collapse varied significantly with treatment (Fig. 8P, Two-way ANOVA treatment | total segment number, $F_{treatment} = 70$, DF = 6, $p < 0.001$). VNC collapse was most penetrant when BMP protein was added just after the birth of the 4d micromere (4q) or 6 or 12 h afterwards (4q+6h and 4q+12h, respectively) and changed every 12 h until stage 6 (cont treatment). The frequency of VNC collapse gradually decreased in animals continuously incubated in BMP protein starting at 4q+18h and 4q+22h, which is just prior to the onset of gastrulation. Adding BMP protein continuously starting at early cleavage stages (1q, 2q, 3q, or 4q) also showed a highly penetrant VNC collapse phenotype (data not shown). Taken together, these data suggest that the critical time window to cause a complete VNC collapse is 12–18 h after birth of the 4d micromere, with some collapse seen with treatment up to the onset of gastrulation (4q+22h). Continuous exposure to BMP protein from gastrulation to stage 6 was

not sufficient to cause a VNC collapse (Fig. 7D). A pulse of BMP protein encompassing 12–18 h after the birth of the 4q micromeres may be sufficient to cause a VNC collapse phenotype; however, this was not tested.

The number and location of segments with either loss of neurotroch cilia or collapsed hemiganglia were scored to look for correlation between these two phenotypes. Segments showing collapsed hemiganglia were significantly more likely to have lost neurotroch cilia (Yang's Chi-Squared test for clustered binary paired data, $X^2 = 9.19$, df = 1, $p = 0.002$), so further analysis only examined hemiganglia collapse. The same trend was evident when examining collapse of the longitudinal nerve tracks in the VNC, but these were highly variable and difficult to quantify (data not shown). The VNC collapse and coincident loss of the neurotroch strongly suggests that the VNC collapse is due to a loss of the ventral midline itself. Two homologs of 'midline markers', *Ct-SIM1* (JGI PID165634) (Denes et al., 2007) and *Ct-ADMP* (JGI PID184506)(Kenny et al., 2014; Scimone et al., 2014) were cloned to confirm midline loss, but neither gene was robustly expressed in the midline of control animals at stage 6 (data not shown).

Eye formation is affected by BMP treatment in a time-dependent manner

There are two larval eyes in *C. teleta*, each composed of three cells: a pigment cell, a sensory cell (SC), and a support cell (Rhode, 1993). The larval eyes degrade during metamorphosis and are replaced by two juvenile or adult eyes. The left larval eye is formed by daughters of blastomere 1a, and the right larval eye is formed by daughters of blastomere 1c (Meyer et al., 2010). BMP treatment had a striking effect on formation of the pigment cells in the larval eyes (Fisher's exact; $p < 0.001$, Fig. 10). The number and position of the larval eye pigment cells in mock-treated animals (both cont and pulse treatments) were not significantly different from animals raised in ASW ($p = 1.0$, data not shown and Fig. 10B, E). Twelve-hour pulses of BMP at 1q, 2q, and 3q generally prevented formation of the larval eye pigment cells (0 eye pigment cells formed, Fig. 10A, E) giving rise to an eyeless phenotype. The 3q pulse had significantly more animals with 'other' eye pigment categories including: 2 larval eye pigment cells not in a wild type configuration or 1 larval eye pigment cell in various locations. A 12-hour pulse of BMP at 4q resulted in 3 larval eye pigment cells; in most animals (66%), the 3rd eye pigment cell was ventromedial ('central eye' Fig. 10C, E) while the next most common phenotype was a ventrolateral 3rd eye pigment cell that was in close proximity to either the left or right larval eye ('stacked eye', 20%, Fig. 6D). There was no left/right bias in which side the stacked ectopic eye pigment cells were located. The proportion of wild-type eye pigment cells increased significantly

and the number of 3 eyes 'stacked' decreased significantly in animals treated with a 12-hour BMP pulse at 4q+6h when compared to a 12-hour BMP pulse at 4q (Fisher's exact post-hoc $p < 0.001$, data not shown). In animals treated with a 12-hour BMP pulse starting at 4q+12h, 4q+18h, or 4q+22h, the larval eye pigment cell phenotype was not significantly different from mock animals. The number of eye pigment cells formed in cont experiments were not significantly different from pulse experiments started at the same stage (2q and 4q cont, Fisher's exact post-hoc $p < 0.1$, data not shown).

Shorter pulse experiments (1 h instead of 12 h) were used to further explore the effect of BMP on larval eye pigment cell formation (Fig 10E). A 1-hour pulse of BMP at 1q produced a range of phenotypes, including 3 larval eye pigment cells (14/37), and a striking right-biased asymmetry where 15/17 animals with two eye pigment cells had both on the right side, and 4/4 animals with 1 eye pigment cell had it on the right side. A 1-hour pulse of BMP at 2q resulted in 0 larval eye pigment cells (36/38). The pattern of eye pigment cells in animals treated with BMP for 1 h at 4q was very similar to the 1q 1 h phenotype: many with 3 eye pigment cells (17/34) and a right-bias with 9/9 two-right eye animals. There were also a number of animals with two ventral eye pigment cells (6/34).

We also examined formation of larval and juvenile eye SCs after BMP treatment (Fig. 11A–D, F–I), both of which are visible during larval stages using a cross-reactive antibody against the *D. melanogaster* protein Futsch (clone 22C10)(Yamaguchi and Seaver, 2013). In wild-type animals, the two larval eye SCs are located at the mediolateral edge of the left and right brain lobes (Fig. 11B, arrows). Each larval eye SC cell has a neurite that extends into the cerebral commissure as well as a bulb-shaped protrusion containing microvilli with f-actin that sits within the cup-shaped pigment cell (Fig 11E), which is characteristic of rhabdomeric photoreceptors (Yamaguchi and Seaver, 2013). The two wild-type juvenile eye SCs are positioned next to the larval eye SCs (Fig. 11G, arrowheads), but are more superficial and have a very different morphology including a process that extends to the surface of the epidermis in the episphere (Fig 11J) and an absence of microvilli with f-actin (Yamaguchi and Seaver, 2013). We quantified the number of larval and juvenile eye SCs after BMP treatment and found different patterns. Larval eye SCs followed the same pattern as the larval eye pigment cells; a 1q pulse of BMP led to 0 SCs, while a 4q pulse led to 3 SCs, most of which were centered. Overall, *C. teleta* formed 0 larval eyes (pigment cells and SCs) with BMP treatments starting at 1q–3q versus 3 larval eyes with treatments starting at 4q; by 4q+12h larval eye formation was wild-type.

In contrast, the juvenile eye SCs increased in number in both 1q and 4q pulse-treated animals (Fig. 11F, H, I). In 1q pulse animals, which did not have larval eye pigment cells or SCs, there were an average of 2.8 ± 0.8SD juvenile eye SCs and a maximum of 5 juvenile eye SCs (Fig. 11F). In 4q pulse animals, all had 3 juvenile eye SCs (Fig. 11F, I). A 1q pulse of BMP increases the number of juvenile SCs, but at 4q, only 3 juvenile SCs are formed, following the pattern of larval eyes. BMP-treated *C. teleta* larvae were not raised through metamorphosis to determine if the juvenile SCs developed into functional eyes.

Serotonergic neurons in the brain are spatially rearranged after BMP treatment

Similar to the larval and juvenile eyes, in *C. teleta* larvae, serotonergic neurons in the brain arise in a bilaterally-symmetric manner, with the same number of 5HT$^+$ soma in each brain lobe at any given stage (Meyer et al., 2015). Since BMP treatment affected the number and location of the larval and juvenile eyes and also appeared to affect the arrangement and number of *Ct-elav1*$^+$ brain lobes depending on the timing of treatment, we scored position of 5HT$^+$ soma in the brain to see if there were similar phenotypes.

Most ASW and mock-treated animals (>82%) had 5HT$^+$ soma that were localized only in the lateral octets of the episphere—the left and right brain lobes (Fig. 12A–D). This corresponded to a symmetric bilateral distribution (ASW: -log likelihood: 56; θ (mean angle(s)): 180° and 0°; κ (concentration): 36 and 12; Mock: -log likelihood: 123; θ: 180°and 0°; κ: 8 and 8). In 1q, 2q, and 3q-treated BMP pulse animals, 5HT$^+$ soma were radially localized—they were found in all regions of the episphere, which best fits a uniform distribution (1q pulse: -log likelihood: 261, 2q pulse: -log likelihood:123, 3q pulse: -log likelihood 103, Fig. 12E–I). Despite the uniform distribution, 3q pulse animals also showed a weak ventral trend. In 4q-treated BMP pulse animals, the 5HT$^+$ soma had a strong ventral distribution, which corresponded to a ventral bimodal distribution (4q pulse: - loglikelihood: 207, θ: 334° and 216°; κ: 2.2 and 4.5, Fig. 12J–L). It is important to note that there is no model to test for a trimodal distribution to statistically confirm the observed three brain lobes, a left, right, and ventral concentration of nuclei in the episphere (e.g. Figs. 6I, 11D). However, we observed 5HT$^+$ soma in the third ectopic brain lobe in 4q-treated BMP pulse animals. Overall, BMP pulses at 1q–3q produce radialized 5HT$^+$ cells, suggesting a radialized brain and a loss of bilateral symmetry in the episphere. At 4q, the statistically determined ventral bimodal pattern likely represents a ventral, trilobed brain.

The ectopic 3rd eye and brain lobe is usually derived from the 1b blastomere

To determine the origin of the third ectopic eye and brain lobe, which were often ventrally localized, we injected the lineage tracer DiI into blastomere 1a or 1b at 1q (8-cell stage) as these

two blastomeres form the ventral quadrants of the episphere (Fig. 13). These embryos were then treated for 12 h with BMP protein starting at 4q. In general, the right eye and the majority of the right brain lobe are formed by the 1c blastomere while the 1a blastomere forms the left eye and a small, ventral region of the left brain lobe. Blastomere 1b normally forms a small, ventral region of the right brain lobe and does not contribute to the two larval eyes (Meyer et al., 2010). Only animals with three eyes (centered or stacked) are discussed here. All (n = 13) 1b-labeled animals with three eyes showed DiI labeling in the ectopic eye (Fig. 13A, B), including two animals with a left stacked ectopic eye and one animal with a right stacked ectopic eye (the remaining 10 animals had a ventral, centered ectopic eye). Interestingly, 3 out of the 10 animals with a centered phenotype also appeared to have DiI labeling in their right eye (Fig. 13B), and both of the animals with the left-stacked phenotype appeared to have DiI labeling in their right eye (total of 5 out of 13; data not shown). It is worth noting that in all of the animals that appeared to have DiI in their right eye in addition to the ectopic eye, the right eye was positioned at the edge of the DiI clone. 1b-injected animals with three eyes also had three brain lobes, and all of these animals had DiI throughout the majority of the ectopic, ventral brain lobe as well as in the normal small, ventral region of the right brain lobe.

Of the animals in which blastomere 1a was labeled with DiI (n=6 with three eyes; 4 centered and 2 stacked), 2 of the 4 centered animals had DiI only in their left eye (Fig. 13C) while the other two had DiI in their left eye as well as in the ectoptic, ventral eye (Fig. 13D). The one animal with a stacked right phenotype had DiI only in the left eye while the one animal with a stacked left phenotype had DiI in the left and the ectopic left eye. 1a-labeled animals with three eyes also had three brain lobes, and in all of these animals, a small, left region of the ventral, ectopic brain lobe was labeled with DiI. This is very similar to how both wild-type brain lobes form, with the majority coming from either 1c or 1d, and a small, ventral region coming from either 1a or 1b (Fig. 13E). In this case, the ectopic brain lobe seems to be primarily generated by 1b with a small, left contribution from 1a (Fig. 13F). Furthermore, these results suggest that 1b primarily forms the ectopic eye (Fig. 13F), but 1a may also be able to contribute to the ectopic eye. Finally, BMP treatment may result in a right eye that is sometimes generated by 1b instead of 1c. These numbers above may be an overestimate because the patchiness of DiI labeling after fixation makes it is difficult to determine if DiI is in the eye cells specifically or simply in the surrounding brain tissue.

Foregut development is disrupted by BMP treatment in a time-dependent manner

Most of the ectodermal tissue in the episphere, including the brain and larval eyes, is generated by 1q micromeres. In order to determine if the dramatic changes after BMP treatment were confined to the episphere, we examined the foregut in the trunk, which is also ectodermal in origin, but is derived from micromeres 2a (left foregut lobe) and 2c (right foregut lobe) (Meyer et al., 2010). The foregut is normally 'butterfly-shaped' with two distinct, separate left and right lobes (Fig. 14A) that eventually fuse at late larval stages to form the foregut. This morphology was notably affected by BMP treatment; foregut shape and ventral maximum surface area were measured to quantify that effect. All control animals (ASW and Mock) showed a normal butterfly-shaped foregut (ASW: n=12, Mock: n=37; Fig. 14A). All animals treated with BMP between 1q and 3q showed a smaller, mostly round foregut (Fig. 14B), with no left-right bias (data not shown). This included both pulse and cont treatments (1q Pulse n=50, 1q Cont n=24, 2q Pulse n=14, 3q Pulse n=28; Fig. 14B). When animals were treated at 4q, the resulting foregut had a distinct 3-lobed, triangular appearance, including both nuclei and foregut cilia (4q pulse, n=25/29, Fig. 14C). The timing to produce a 3-lobed foregut was precise, and animals treated too early would generally have a small, round foregut similar to the 1q–3q phenotype (data not shown). Animals treated after 4q had a generally normal bilobed foregut (data not shown). The foreguts of 1q, 2q, 3q, and 4q pulse BMP-treated animals had significantly smaller ventral surface areas than control animals (Fig. 14D, E; ANOVA [ASW, Mock, 1q Pulse, 2q Pulse, 3q Pulse], $F_{treatment} = 12.0$, DF = 4, $p < 0.001$; ANOVA [Mock, 4q Pulse], $F_{treatment} = 5.9$, DF = 1, $p = 0.026$). Foregut sizes for 1q, 2q, and 3q pulse animals were not significantly different from each other (Tukey HSD, $p > 0.92$). Overall, 1q, 2q, and 3q BMP pulse-treated animals had a reduced, radial foregut, while 4q pulse animals had a tri-lobed foregut (Fig. 14B, C).

Discussion

Although BMP signaling plays many roles during development, we focused on neural fate specification for the brain and VNC. Unlike the function of BMPs to limit neural specification in vertebrates and insects, our results demonstrate that ectopic BMP in the annelid *C. teleta* is not sufficient to block formation of the brain or VNC, nor does it affect overall formation of the D-V axis, suggesting that it does not act as an organizer signal. We observed a number of distinct and penetrant phenotypes that clustered into three groups depending on the time window of BMP application (Fig. 15). 1) A loss or reduction of larval eyes, brain lobes, and foregut was a dominant phenotype that appears to be due to exogenous BMP during an ~1 h time window

after the birth of 2d (1q–3q 12 h pulses would all at least partially overlap this window). 2) A third ectopic eye, brain lobe, and foregut lobe are formed by exogenous BMP exposure between ~0–6 h after birth of 4q until ~12 h after birth of 4q. 3) A loss of the ventral midline (neurotroch ciliary band) and a collapse of the VNC produced by ectopic BMP exposure between ~4q+12 h and 4q+22 h (i.e. several hours prior to the onset of gastrulation).

BMP signaling in *C. teleta* may induce quadrant-specific blastomere fates

We hypothesize that BMP signaling induces blastomere fates in a timing-dependent manner in *C. teleta*. Like many spiralians, *C. teleta* has a stereotyped cleavage pattern, where cell fates are predetermined by regulated cell division (Meyer et al., 2010). The four quadrants of the episphere are formed by descendants of micromeres 1a–1d, and the left and right brain lobes are primarily generated by $1c^1$ and $1d^1$ with minor contributions to the ventral side of each brain lobe from $1a^1$ and $1b^1$ (Fig13E). The left and right eyes are generated by $1a^1$ and $1c^1$. The majority of the left and right lobes of the foregut, which will form the pharynx and esophagus, are generated by micromeres 2a and 2c with minor contributions to the region between the two foregut lobes from 2b, 3a, 3b, and 3d. Furthermore, the mouth or stomodeum is generated by 2a–2c and 3a–3d with surface cells around the mouth opening coming from 2d.

The D-quadrant is of particular interest for early developmental signaling because the D-quadrant produces the organizer in spiralians (Henry et al., 2017). The organizer is the cell(s) responsible for setting up the D-V axis by signaling to adjacent cells in the early embryo (Lambert and Nagy, 2002). In the annelid *Capitella teleta*, one cell at the 13- to 16-cell stage (blastomere 2d) has been reported to be the organizer (Amiel et al., 2013), and descendants of 2d form the trunk and pygidial ectoderm, including the VNC (Meyer and Seaver, 2010). Blastomere ablation experiments demonstrated that 2d is necessary for D-V axis specification in the episphere and for mesoderm induction in the trunk (Amiel et al., 2013). Furthermore, drug studies on *Capitella teleta* and another annelid, *Chaetopterus pergamentaceus*, suggest that an Activin/Nodal but not BMP or FGF/MAPK signal organizes the D-V axis during the same time window when 2d is present (Lanza and Seaver, 2020b, 2020a). Finally, blastomere isolations on *C. teleta* have shown that formation of the VNC but not the brain relies on signals from the macromeres during the time window when 2d is acting as an organizer (Carrillo-Baltodano and Meyer, 2017). However, results from these experiments suggest that D-V axis formation occurs independently of VNC induction (Carrillo-Baltodano, 2019, in prep). These data raise the questions for annelids of what signals induce neural fate, whether similar or different genetic

pathways act during VNC and brain formation, and whether or not neural induction is linked with D-V axis formation as it is in insects and vertebrates.

In wild-type *C. teleta* embryos, A- and C-quadrant micromeres are positioned on either side of the D-quadrant, while B-quadrant micromeres are positioned farther away from the D-quadrant, on the opposite side of the embryo. The D-quadrant macromere divides first during each cleavage, followed by the C-, then B-, and finally A-quadrant macromeres. Based on our results, we hypothesize that BMP signaling from the D-quadrant acts first on D-quadrant micromeres as they are born (with early, high, and/or autonomous levels of BMP signaling). Subsequently, the neighboring C- and A-quadrant micromeres are born, receiving later and/or lower juxtacrine BMP signaling. The B-quadrant micromeres, which are the farthest away from the D-quadrant, may adopt their fates in the absence of BMP signaling. mRNA transcripts for many proteins in the BMP pathway are present during early cleavage stages (Lanza and Seaver, 2020a, Webster et al in prep) Furthermore, data from *C. teleta* (Lanza and Seaver, 2020b, Webster et al. in prep)*, Tritia obsoleta* (Lambert et al., 2016; Lambert and Nagy, 2002), and *Crepidula fornicata* (Lyons et al., 2020) all show either increased BMP signaling through pSMAD1/5/8 or variation in when mRNA appears in the D-quadrant relative to the other quadrants. However, localization of ligands and antagonists does not necessarily predict where the pathway is active. In order to test where BMP signaling is normally active, we extensively tested multiple anti-pSMAD1/5/8 antibodies under several different conditions in *C. teleta*; however, we were not able to get nuclear staining. It is unclear if this is related to the truncation of SMAD1/5/8.

We hypothesize based on the data presented here that adding exogenous BMP protein around the same time as birth of the 2d organizer cell causes the 1a–1c micromeres (or their daughters) to adopt a 1d fate. This would result in a radialized brain with ectopic neural tissue and no larval eyes—which is what we observe. This same time window produces extra juveniles eye SCs, which arise from descendants of 1a and 1c (Yamaguchi and Seaver, 2013), but we were not able to infer how excess BMP protein or fate switching may play a role as the development of juvenile eyes is not well understood. The reduced foregut may also represent a loss of some A and C-quadrant fates as the D-quadrant largely does not contribute to the foregut. However, our phenotypes do not seem to be consistent with a gain of a D-quadrant fates since some foregut tissue appears to be present, although this should be tested with a molecular marker such as *Ct-foxA* (Boyle and Seaver, 2008), and the trunk ectoderm including VNC is fairly intact (2d derivatives). We suggest this could be explained by differences in specification between the episphere and the trunk, including the role of BMP signaling (Carrillo-Baltodano and Meyer, 2017). Alternatively,

2a and 2c may only partially adopt a 2d fate, making reduced contributions to the foregut, as wild-type 2d does not contribute to the foregut.

We hypothesize that adding BMP after the birth of 4d (until a few hours later) may cause B-quadrant micromeres to adopt a C-quadrant fate, causing 1b to produce a third, ectopic, ventral eye, juvenile SC and brain lobe, while 2b produces an ectopic medial foregut lobe (phenotype 2, above). We found that the third, ectopic, ventral eye and brain lobe are formed primarily by the 1b lineage, with minor contributions from 1a, although contributions from 1c and 1d were not assessed (Fig. 13).

There is support for the BMP fate switching hypothesis in the mollusc *Tritia (=Ilyanassa) obsoleta,* where a 2b lineage-specific gene *To-2b* has been identified (Lambert et al., 2016). After knockdown with a BMP morpholino, *To-2b* was present in all four blastomere lineages, suggesting a fate switch where A, C, and D all adopted a B fate. Furthermore, after adding BMP, pSMAD activity appeared in 1b, suggesting it was now receiving BMP signaling (Lambert et al., 2016). Switching the fate of 1b fate also caused a collapse of the episphere midline in *T. obsoleta* (Clement, 1967); if there is a loss of episphere midline tissue in *C. teleta* as well, that could explain the displacement of some eyes in the 'stacked' eye phenotype. A role of BMP in fate changing was also suggested for *Helobdella sp* Austin, where a BMP2/4 morpholino caused the P bandlet to take on a O fate (Kuo and Weisblat, 2011).

The loss of the midline (phenotype 3, above) does not fit with a blastomere fate transition paradigm, although we are lacking lineage tracing data for the relevant time period (after 4q+12 h) to identify the specific cells involved. The ventral midline in *C. teleta* larvae largely consists of ciliated neurotroch cells that arise from descendants of $2d^{12}$ and $2d^{2}$, and these cells appear to be lost after continuous BMP treatment. There are also ciliated cells around the mouth that are formed by descendants of 3c and 3d (Meyer et al., 2010), and these cells appear unaffected by continuous BMP treatment. $2d^{12}$ and $2d^{2}$ are also responsible for formation of the pygidial ectoderm, telotroch and peripheral nerves which were also unaffected. If the specific cells responsible for delineating the ventral midline separate from the other daughter cells ~12–18 h after the fourth quartet (e.g. $2d^{121}$), loss of those fates could explain the midline collapse. Alternatively, the midline collapse could relate to ectodermal D-V fates, where the dorsal expansion of *Ct-chrdl* would be associated with a ventral loss of the midline. This is not unreasonable; the *Ct-chrdl* expansion in continuous treatments was 25.4 μm ± 19.8 μm (SD), while the average reduction in *Ct-elav1* domain in continuous treatments was 17.3 μm ± 14.4 μm (SD), although this is only true for segment 4.

Our data supports a role for BMP in fate switching in the episphere during early cleavage; here we either caused A- and C-quadrants to have a D fate around 2q, or the B-quadrant to adopt an A- or C-fate after 4q.

BMP signaling in Spiralia has varied effects

Our results showed no effect of added BMP on overall D-V axis formation but instead highlighted distinct effects on fates arising from blastomeres in each of the quadrants, including neural tissue in the head. Lanza and Seaver (2018) tested the BMP pathway inhibitor dorsomorphin dihydrochloride, which inhibits the BMP receptor ALK2/3, on 4-cell to 32-cell (~3q) *C. teleta* embryos. They found four separate phenotypes with a gradual reduction of features, from relatively wild-type to small disorganized balls with an episphere but no trunk. ~75% of the treated larvae had A-P and D-V axes including a brain and VNC while ~25% of the treated larvae were small, disorganized balls with anterior features including a putative brain (radial) and a single ciliary band, but no trunk, VNC, or foregut. Specific neural phenotypes were not described in detail. Lanza and Seaver (2020b) also tested the effect of SMAD1/5/8 morpholinos in *C. teleta*, and found a milder phenotype than with dorsomorphin: the vast majority of larvae had all three body axes including two eyes and brain lobes (~90%), many of which were wild-type-like, but many of which also showed a disrupted VNC and/or neurotroch.

The function of BMP signaling in ectodermal and neural development has been examined in nine spiralian species to date. Within Pleistoannelida (Errantia + Sedentaria), three taxa have been examined: *C. teleta*, *Helobdella sp*. Austin, and *Platynereis dumerilii* (Struck, 2011). In *Helobdella sp*. Austin, gain- and loss-of-function experiments demonstrated that BMPs are important for D-V patterning of the ectoderm within the midbody and caudal segments; however, no effects on neural induction or the overall D-V axis including the mesoderm were reported (Kuo et al., 2012; Kuo and Weisblat, 2011). These studies focused on later functions of BMP signaling in ectodermal patterning. In general, knocking down *Hau-bmp5-8* caused a ventralization of the ectoderm, while adding ectopic BMP5-8 mRNA caused a dorsalization of the ectoderm. This matches with our results where exogenous BMP4 treatment caused a dorsal expansion of *Ct-chrdl* expression in the ectoderm. In *P. dumerilii*, the function of BMP was investigated later, during neural patterning (Denes et al., 2007), where a short exposure to BMP protein did not affect *Pdu-elav* expression, as was the case for *C. teleta*. Instead, application of exogenous recombinant BMP4 protein during development affected ectodermal D-V patterning but did not repress neural induction or affect the overall formation of the D-V axis (Denes et al., 2007). In another annelid *Chaetopterus pergamentaceus*, which is in a sister-clade to all

annelids except Oweniidae and Magelonidae (Weigert et al., 2014), inhibition of BMP with DMH1 or dorsomorphin during early cleavage stages showed no resulting phenotype (Lanza and Seaver, 2020a).

In the brachiopods *Novocrania anomala* and *Terebratalia transversa* (Martín-Durán et al., 2016), DMH1 (dorsomorphin homolog 1; inhibits the ALK2 BMP receptor) caused an expansion of some ventral genes, as well as an expansion of anterior genes and reduction of posterior genes; knocking down BMP affected both D-V and A-P axis marker genes (Table 1). Four spiralian species, *C. teleta* (this study), *Tritia obsoleta* (Lambert et al., 2016), *Crepidula fornicata* (Lyons et al., 2020) and *Lottia goshimai* (Tan et al., 2020), were studied at early stages of development and show striking similarities and differences in phenotypic effects of BMP (Table 1).

Direct comparisons of the four species where recombinant BMP4 protein was added during early cleavage stages showed phenotypes in the episphere with very little disruption of trunk development. The exception was *L. goshimai* where only eye morphology was discussed after adding BMP. All four species showed changes in the number of eyes although the number and positioning of ectopic eyes varied. Interestingly, the resulting phenotype from treating with BMP ~1q-3q was most similar between *Ca. teleta* and *Cr. fornicata*, while *Tr. obsoleta* showed an opposite result. For example, reduction and radialization of neural tissue in the episphere was seen in *Ca. teleta* and *Cr. fornicata* (reduced $5HT^+$ neurons vs episphere pinching off), whereas *Tr. obsoleta* showed an increase in neural tissue. Lambert et al. (2016) did not test later cleavage effects, however the increase in neural tissue and ectopic eyes seen in Tr. obsoleta at 1q-3q is similar to the effect in both *Ca. teleta* and *Cr. fornicata* at the 4q- (~64-cell) stage.

Overall, the role of BMP in spiralians is a variation on a common theme. Neural tissue in the episphere is more likely to be affected than neural tissue in the trunk, although whether the brain is expanded or reduced upon BMP exposure varies (Table 1). The function of BMP signaling in D-V axis formation and organizer activity is also highly variable, although many species showed an expansion of ventral fates with a knockdown of BMP. How the function of BMP in development has evolved in spiralians remains to be seen, and could give some interesting insight into how the stereotyped cleavage of many spiralians can lead to systems drift or other forms of genetic evolution.

BMP signaling does not establish the D-V axis in *C. teleta*

Our results show no overarching role of BMP signaling in establishing the D-V axis; specifically, we found no loss of the D-V axis after treatment with ectopic BMP protein. The function of BMP

signaling in D-V axis formation is well characterized in vertebrates and insects (De Robertis, 2008), and a role for BMP in organizer signaling and/or D-V axis formation has been shown in three spiralians, *Tr. obsoleta* (Lambert et al., 2016), *L. goshimai* (Tan et al., 2020), and *Crassotrea gigas* (Tan et al., 2018), and during regeneration in *Dugesia japonica* (Orii and Watanabe, 2007). Although we saw an expansion of the dorsal domain of *Ct-chrdl* in the ectoderm, no D-V axis disruption was seen in BMP-treated animals, supporting our conclusion that BMP signaling is not a key feature of D-V axis formation nor organizer signaling in *C. teleta*. Because of the differences between vertebrate development and spiral cleavage, how an organizer functions in each group may vary. If BMP signaling is important for establishing the quadrant identities of early blastomeres in *C. teleta*, this may be a type of early organizing activity, but one that is specific to development within a spiral cleavage program. Further examination of BMP signaling in the context of spiralian organizer signaling and spiral cleavage is warranted, especially in additional species to understand how the function of BMP has evolved across this diverse group of animals.

BMP does not block neural specification in *C. teleta*

Data from other spiralians (Table 1) support our conclusion that BMP signaling plays an important role in brain formation, but does not appear to block neural specification in Spiralia as in vertebrates and insects. Furthermore, work by Carrillo-Baltodano and Meyer (2017) suggests that neural tissue in the episphere can be autonomously specified, while specification of the VNC in the trunk requires inductive signaling from the vegetal macromeres (Carrillo-Baltodano and Meyer, 2017). Their blastomere isolations showed that the 1q micromeres are capable of making neural tissue in isolation, although without a clear D-V axis. Here we show that daughters of 1b are capable of making additional neural tissue when exposed to ectopic BMP signaling for 12 h starting at 4q. It is possible that descendants of 1b autonomously produce neural tissue, but that this contribution is limited to a small region of the right-ventral brain as a result of conditional signaling. Our results support the hypothesis that neural specification occurs via two different modes in the episphere and trunk of *C. teleta* and suggests that neural specification of the brain and VNC does not occur via inhibition of BMP signaling.

Our results align with multiple lines of evidence across Bilateria showing that the function of BMP signaling in neural induction is not conserved across Bilateria (Martín-Durán et al., 2018; Zhao et al., 2019). For example, in vertebrates, formation of the dorsal neural tube relies in part on inhibition of BMP signaling by graded antagonists secreted from the organizer (e.g. Chordin, Noggin, and Follistatin) but other signals such as FGFs (via the MAPK cascade) and Wnts are

also important (De Robertis and Kuroda, 2004; Stern, 2006, 2005; Wilson and Edlund, 2001). Grafting and drug experiments in the lancelet (a sister-clade to vertebrates) *Branchiostoma laceleolatum* suggest that the main organizer signal and neural inducer is Nodal/Activin, not BMP antagonists (Le Petillon et al., 2017); however, disrupting BMP signaling affects both the D-V axis and neural induction in *B. floridae* and *Branchiostoma lanceolatum*. Further complicating the evolutionary picture are data from hemichordates—non-chordate deuterostomes with a neural plexus and dorsal and ventral nerve cords in at least some taxa (Cunningham and Casey, 2014; Lowe et al., 2003; Nomaksteinsky et al., 2009). In the hemichordate *Saccoglossus kowalevskii*, exogenous BMPs dorsalize the animal but do not repress neural induction (Lowe et al., 2006) while knockdown of an *fgf8/17/18* homolog blocks mesoderm specification; however, no effect on neural fate specification was reported (Green et al., 2013).

Data from the insects *Drosophila melanogaster* and *Tribolium castaneum* suggest that BMP signaling and activation of MAPK signaling are involved in D-V axis specification and in delimiting the neuroectoderm (Chen et al., 2000; Irish and Gelbart, 1987; Lynch and Roth, 2011; Nunes da Fonseca et al., 2008; van der Zee et al., 2006; von Ohlen and Doe, 2000; Wheeler et al., 2005; Wilson et al., 2014), similar to the function in vertebrates. There are fewer data from non-insect arthropods, but in the spider *Achaearanea tepidariorum*, knockdown of the BMP antagonist Sog led to a complete loss of the CNS and ventral fates (Akiyama-Oda and Oda, 2006), suggesting a possible conservation of BMP/Dpp function in D-V axis formation and delimitation of the ventral neuroectoderm in arthropods. Function of BMP signaling in D-V axis formation and neural induction across Ecdysozoa is less consistent (Zhao et al., 2019). In the onychophoran *Euperipatoides rowelli, dpp* expression differs from any other examined panarthropod, strongly suggesting a divergent role in development (Treffkorn and Mayer, 2013). Further removed is the role of BMP homologs in nematodes, where they do not appear to play a role in early developmental patterning in *C. elegans* (Patterson and Padgett, 2000).

The lack of a conserved function of BMP signaling in neural induction across Bilateria has deep implications for our understanding of the evolution of nervous systems and CNSs across Bilateria, although further data, especially broader phylogenetic sampling is required to make any conclusions (Martín-Durán and Hejnol, 2019).

Conclusions

Adding exogenous BMP protein to early-cleaving *C. teleta* embryos had a striking effect on formation of the brain, eyes, and foregut in a time-dependent manner. However, adding BMP

did not block neural specification of the brain or VNC or block formation of the D-V axis at any of the treatment time windows. These data combined with those from other non-insect and vertebrate taxa question whether BMP signaling was involved in these two processes in the last common ancestor of Bilateria. Rather, we identified three key time windows of BMP activity in *C. teleta*. First, early treatment around 2q caused the loss of the eyes, radialization of the brain, and a reduction of the foregut, which we interpret as a loss of A-, B- and C-quadrant identities and possibly a trans-fate switch to a D-quadrant identity. Later treatment after 4q was able to induce formation of an ectopic brain lobe and eye, which we interpret as a trans-fate switch of the B-quadrant to a C-quadrant identity. Thirdly, while the D-V axis in the trunk was largely unaffected by any of the BMP treatment windows, continuous BMP treatment from early cleavage through mid-larval stages resulted in a modest expansion of *Ct-chrdl* expression in the dorsal ectoderm and a concomitant loss of the ventral midline (neurotroch ciliary band) and a collapse of the bilaterally-symmetric VNC. Strikingly, there was little to no reduction in neural tissue in the VNC after these continuous BMP treatments. Our results, in conjunction with data from other annelids and molluscs suggest that BMP signaling was not ancestrally involved in delimiting neural tissue or establishing the D-V axis in the last common ancestor of annelids. However, the effects ectopic BMP on quadrant-identity during cleavage stages may represent a very early 'organizing' function in the context of spiralian development. Ultimately, studies on a wider range of spiralian taxa are needed to determine if the ability of BMP signaling to block neural induction and help establish the D-V axis was lost within Annelida or if BMP signaling gained these functions multiple times across Bilateria. Ultimately, these comparisons will give us insight into the evolutionary origins of centralized nervous systems and body plans.

Acknowledgements

The authors thank R. Bellin at the College of the Holy Cross for access to the confocal microscope.

Funding

This work was supported by the National Science Foundation [Continuing grant #1656378]

References

Akiyama-Oda, Y., Oda, H., 2006. Axis specification in the spider embryo: *dpp* is required for radial-to-axial symmetry transformation and *sog* for ventral patterning. Development 133, 2347–2357. https://doi.org/10.1242/dev.02400

Amiel, A.R., Henry, J.Q., Seaver, E.C., 2013. An organizing activity is required for head patterning and cell fate specification in the polychaete annelid *Capitella teleta*: New

insights into cell–cell signaling in Lophotrochozoa. Dev Biol 379, 107–122. https://doi.org/10.1016/j.ydbio.2013.04.011

Arendt, D., Denes, A.S., Jekely, G., Tessmar-Raible, K., 2008. The evolution of nervous system centralization. Philos Trans R Soc Lond B Biol Sci 363, 1523–8. https://doi.org/H509L18055200QNJ [pii] 10.1098/rstb.2007.2242

Blake, J.A., Grassle, J.P., Eckelbarger, K.J., 2009. *Capitella teleta*, a new species designation for the opportunistic and experimental *Capitella sp*. I, with a review of the literature for confirmed records. Zoosymposia 2, 25–53.

Boyle, M.J., Seaver, E.C., 2008. Developmental expression of foxA and gata genes during gut formation in the polychaete annelid, Capitella sp. I. Evolution & Development 10, 89–105. https://doi.org/10.1111/j.1525-142X.2007.00216.x

Branam, A.M., Hoffman, G.G., Pelegri, F., Greenspan, D.S., 2010. Zebrafish *Chordin-like* and *Chordin* Are Functionally Redundant in Regulating Patterning of the Dorsoventral Axis. Dev Biol 341, 444–458. https://doi.org/10.1016/j.ydbio.2010.03.001

Carrillo-Baltodano, A.M., 2019. Understanding the evolution of animal body plans by looking at annelid neural development (PhD). Clark University, Worcester, MA.

Carrillo-Baltodano, A.M., Meyer, N.P., 2017. Decoupling brain from nerve cord development in the annelid *Capitella teleta*: Insights into the evolution of nervous systems. Dev Biol 431, 134–144. https://doi.org/10.1016/j.ydbio.2017.09.022

Chen, G., Handel, K., Roth, S., 2000. The maternal N*F-kappaB/dorsal* gradient of *Tribolium castaneum*: dynamics of early dorsoventral patterning in a short-germ beetle. Development 127, 5145–5156.

Clement, A.C., 1967. The embryonic value of the micromeres in *Ilyanassa obsoleta*, as determined by deletion experiments. I. The first quartet cells. Journal of Experimental Zoology 166, 77–88. https://doi.org/10.1002/jez.1401660109

Cunningham, D., Casey, E.S., 2014. Spatiotemporal development of the embryonic nervous system of *Saccoglossus kowalevskii*. Dev Biol 386, 252–63. https://doi.org/10.1016/j.ydbio.2013.12.001

Davis, G.K., D'Alessio, J.A., Patel, N.H., 2005. Pax3/7 genes reveal conservation and divergence in the arthropod segmentation hierarchy. Developmental Biology 285, 169–184. https://doi.org/10.1016/j.ydbio.2005.06.014

De Robertis, E.M., 2008. Evo-Devo: Variations on Ancestral Themes. Cell 132, 185–195. https://doi.org/10.1016/j.cell.2008.01.003

De Robertis, E.M., Kuroda, H., 2004. Dorsal-ventral patterning and neural induction in *Xenopus* embryos. Annu Rev Cell Dev Biol 20, 285–308. https://doi.org/10.1146/annurev.cellbio.20.011403.154124

Denes, A.S., Jékely, G., Steinmetz, P.R.H., Raible, F., Snyman, H., Prud'homme, B., Ferrier, D.E.K., Balavoine, G., Arendt, D., 2007. Molecular Architecture of Annelid Nerve Cord Supports Common Origin of Nervous System Centralization in Bilateria. Cell 129, 277–288. https://doi.org/10.1016/j.cell.2007.02.040

Fitak, R.R., Johnsen, S., 2017. Bringing the analysis of animal orientation data full circle: model-based approaches with maximum likelihood. J Exp Biol 220, 3878–3882. https://doi.org/10.1242/jeb.167056

Gámez, B., Rodriguez-Carballo, E., Ventura, F., 2013. BMP signaling in telencephalic neural cell specification and maturation. Frontiers in Cellular Neuroscience 7. https://doi.org/10.3389/fncel.2013.00087

Giribet, G., Dunn, C.W., Edgecombe, G.D., Hejnol, A., Martindale, M.Q., Rouse, G.W., 2009. Assembling the spiralian tree of life, in: Telford, M.J. and D.T.J.L. (Ed.), Animal Evolution: Genomes, Fossils, and Trees. Oxford University Press, Oxford, pp. 52–64.

Grassle, J., Grassle, J.F., 1976. Sibling species in the marine pollution indicator *Capitella* (polychaeta). Science 192, 567–569. https://doi.org/10.1126/science.1257794

Green, S.A., Norris, R.P., Terasaki, M., Lowe, C.J., 2013. FGF signaling induces mesoderm in the hemichordate *Saccoglossus kowalevskii*. Development 140, 1024–33. https://doi.org/10.1242/dev.083790

H. Wickham, 2009. ggplot2: Elegant Graphics for Data Analysis. Springer-Verlag, New York.

Hejnol, A., Rentzsch, F., 2015. Neural nets. Current Biology 25, R782–R786. https://doi.org/10.1016/j.cub.2015.08.001

Heldin, C.-H., Miyazono, K., ten Dijke, P., 1997. TGF-β signalling from cell membrane to nucleus through SMAD proteins. Nature 390, 465–471. https://doi.org/10.1038/37284

Helm, C., Beckers, P., Bartolomaeus, T., Drukewitz, S.H., Kourtesis, I., Weigert, A., Purschke, G., Worsaae, K., Struck, T.H., Bleidorn, C., 2018. Convergent evolution of the ladder-like ventral nerve cord in Annelida. Front. Zool. 15, 36. https://doi.org/10.1186/s12983-018-0280-y

Henry, J.Q., Lyons, D.C., Perry, K.J., Cornelia Osborne, C., 2017. Establishment and activity of the D quadrant organizer in the marine gastropod *Crepidula fornicata*. Dev Biol. https://doi.org/10.1016/j.ydbio.2017.09.003

Holland, N.D., 2003. Early central nervous system evolution: an era of skin brains? Nat Rev Neurosci 4, 617–27.

Holley, S.A., Jackson, P.D., Sasai, Y., Lu, B., al, et, 1995. A conserved system for dorsal-ventral patterning in insects and vertebrates involving *sog* and *chordin*. Nature; London 376, 249–53.

Irish, V.F., Gelbart, W.M., 1987. The *decapentaplegic* gene is required for dorsal-ventral patterning of the *Drosophila* embryo. Genes & Development 1, 868–879. https://doi.org/10.1101/gad.1.8.868

Kenny, N.J., Namigai, E.K.O., Dearden, P.K., Hui, J.H.L., Grande, C., Shimeld, S.M., 2014. The Lophotrochozoan TGF-β signalling cassette - diversification and conservation in a key signalling pathway. The International Journal of Developmental Biology 58, 533–549. https://doi.org/10.1387/ijdb.140080nk

Kocot, K.M., Struck, T.H., Merkel, J., Waits, D.S., Todt, C., Brannock, P.M., Weese, D.A., Cannon, J.T., Moroz, L.L., Lieb, B., Halanych, K.M., 2016. Phylogenomics of Lophotrochozoa with consideration of systematic error. Syst Biol 66, syw079-. https://doi.org/10.1093/sysbio/syw079

Kuo, D.-H., Shankland, M., Weisblat, D.A., 2012. Regional differences in BMP-dependence of dorsoventral patterning in the leech *Helobdella*. Dev Biol 368, 86–94. https://doi.org/10.1016/j.ydbio.2012.05.021

Kuo, D.-H., Weisblat, D.A., 2011. A New Molecular Logic for BMP-Mediated Dorsoventral Patterning in the Leech *Helobdella*. Current Biology 21, 1282–1288. https://doi.org/10.1016/j.cub.2011.06.024

Lambert, J.D., Johnson, A.B., Hudson, C.N., Chan, A., 2016. Dpp/BMP2-4 Mediates Signaling from the D-Quadrant Organizer in a Spiralian Embryo. Current Biology 26, 2003–2010. https://doi.org/10.1016/j.cub.2016.05.059

Lambert, J.D., Nagy, L.M., 2002. Asymmetric inheritance of centrosomally localized mRNAs during embryonic cleavages. Nature 420, 682–686. https://doi.org/10.1038/nature01241

Lanza, A.R., Seaver, E.C., 2020a. Activin/Nodal signaling mediates dorsal–ventral axis formation before third quartet formation in embryos of the annelid Chaetopterus pergamentaceus. EvoDevo 11, 17. https://doi.org/10.1186/s13227-020-00161-y

Lanza, A.R., Seaver, E.C., 2020b. Functional evidence that Activin/Nodal signaling is required for establishing the dorsal-ventral axis in the annelid *Capitella teleta*. Development 147, dev189373. https://doi.org/10.1242/dev.189373

Le Petillon, Y., Luxardi, G., Scerbo, P., Cibois, M., Leon, A., Subirana, L., Irimia, M., Kodjabachian, L., Escriva, H., Bertrand, S., 2017. Nodal–Activin pathway is a conserved

neural induction signal in chordates. Nature Ecology & Evolution 1, 1192–1200. https://doi.org/10.1038/s41559-017-0226-3

Lowe, C.J., Terasaki, M., Wu, M., Jr, R.M.F., Runft, L., Kwan, K., Haigo, S., Aronowicz, J., Lander, E., Gruber, C., Smith, M., Kirschner, M., Gerhart, J., 2006. Dorsoventral Patterning in Hemichordates: Insights into Early Chordate Evolution. PLOS Biology 4, e291. https://doi.org/10.1371/journal.pbio.0040291

Lowe, C.J., Wu, M., Salic, A., Evans, L., Lander, E., Stange-Thomann, N., Gruber, C.E., Gerhart, J., Kirschner, M., 2003. Anteroposterior patterning in hemichordates and the origins of the chordate nervous system. Cell 113, 853–65. https://doi.org/S0092867403004690 [pii]

Lynch, J.A., Roth, S., 2011. The evolution of dorsal-ventral patterning mechanisms in insects. Genes & Development 25, 107–118. https://doi.org/10.1101/gad.2010711

Lyons, D.C., Perry, K.J., Batzel, G., Henry, J.Q., 2020. BMP signaling plays a role in anterior-neural/head development, but not organizer activity, in the gastropod *Crepidula fornicata*. Developmental Biology 463, 135–157. https://doi.org/10.1016/j.ydbio.2020.04.008

Mangiafico, S.S., 2015. An R Companion for the Handbook of Biological Statistics, version 1.3.2. rcompanion.org/rcompanion/.

Martín-Durán, J.M., Hejnol, A., 2019. A developmental perspective on the evolution of the nervous system. Developmental Biology. https://doi.org/10.1016/j.ydbio.2019.10.003

Martín-Durán, J.M., Pang, K., Børve, A., Lê, H.S., Furu, A., Cannon, J.T., Jondelius, U., Hejnol, A., 2018. Convergent evolution of bilaterian nerve cords. Nature 553, 45–50. https://doi.org/10.1038/nature25030

Martín-Durán, J.M., Passamaneck, Y.J., Martindale, M.Q., Hejnol, A., 2016. The developmental basis for the recurrent evolution of deuterostomy and protostomy. Nature Ecology & Evolution 1, s41559-016-0005–0016. https://doi.org/10.1038/s41559-016-0005

Meyer, N.P., Boyle, M.J., Martindale, M.Q., Seaver, E.C., 2010. A comprehensive fate map by intracellular injection of identified blastomeres in the marine polychaete *Capitella teleta* . EvoDevo 1, 8. https://doi.org/10.1186/2041-9139-1-8

Meyer, N.P., Carrillo-Baltodano, A., Moore, R.E., Seaver, E.C., 2015. Nervous system development in lecithotrophic larval and juvenile stages of the annelid *Capitella teleta*. Front. Zool. 12, 27. https://doi.org/10.1186/s12983-015-0108-y

Meyer, N.P., Seaver, E.C., 2010. Cell Lineage and Fate Map of the Primary Somatoblast of the Polychaete Annelid *Capitella teleta*. Integr Comp Biol 50, 756–767. https://doi.org/10.1093/icb/icq120

Meyer, N.P., Seaver, E.C., 2009. Neurogenesis in an annelid: Characterization of brain neural precursors in the polychaete *Capitella* sp. I. Dev Biol 335, 237–252. https://doi.org/10.1016/j.ydbio.2009.06.017

Muller, M.C., 2006. Polychaete nervous systems: Ground pattern and variations--cLS microscopy and the importance of novel characteristics in phylogenetic analysis. Integr. Comp. Biol. 46, 125–33. https://doi.org/10.1093/icb/icj017

Nielsen, C., 2005. Larval and adult brains. Evolution & Development 7, 483–489. https://doi.org/10.1111/j.1525-142X.2005.05051.x

Nomaksteinsky, M., Rottinger, E., Dufour, H.D., Chettouh, Z., Lowe, C.J., Martindale, M.Q., Brunet, J.F., 2009. Centralization of the deuterostome nervous system predates chordates. Curr Biol 19, 1264–9. https://doi.org/10.1016/j.cub.2009.05.063

Nunes da Fonseca, R., von Levetzow, C., Kalscheuer, P., Basal, A., van der Zee, M., Roth, S., 2008. Self-regulatory circuits in dorsoventral axis formation of the short-germ beetle Tribolium castaneum. Dev Cell 14, 605–15. https://doi.org/10.1016/j.devcel.2008.02.011

Orii, H., Watanabe, K., 2007. Bone morphogenetic protein is required for dorso-ventral patterning in the planarian *Dugesia japonica*. Dev Growth Differ 49, 345–9. https://doi.org/10.1111/j.1440-169X.2007.00931.x

Patterson, G.I., Padgett, R.W., 2000. TGFβ-related pathways: roles in Caenorhabditis elegans development. Trends in Genetics 16, 27–33. https://doi.org/10.1016/S0168-9525(99)01916-2

R Core team, 2014. R: A language and environment for statistical computing. R Foundation for Statistical Computing., Vienna, Austria.

Rhode, B., 1993. Larval and adult eyes in *Capitella spec. I* (Annelida, Polychaeta). J Morphol 217, 327–335.

RStudio Team, 2012. RStudio : Integrated Development for R. RStudio, Inc. [Online]. RStudio. Available: http://www.rstudio.org/ [2015, August 28]. RStudio, Boston, MA.

Schindelin, J., Arganda-Carreras, I., Frise, E., Kaynig, V., Longair, M., Pietzsch, T., Preibisch, S., Rueden, C., Saalfeld, S., Schmid, B., Tinevez, J.-Y., White, D.J., Hartenstein, V., Eliceiri, K., Tomancak, P., Cardona, A., 2012. Fiji: an open-source platform for biological-image analysis. Nature Methods 9, 676–682. https://doi.org/10.1038/nmeth.2019

Schmidt-Rhaesa, A., Harzsch, S., Purschke, G., 2015. Structure and Evolution of Invertebrate Nervous Systems. Oxford University Press. https://doi.org/10.1093/acprof:oso/9780199682201.001.0001

Scimone, M.L., Lapan, S.W., Reddien, P.W., 2014. A forkhead Transcription Factor Is Wound-Induced at the Planarian Midline and Required for Anterior Pole Regeneration. PLoS Genet 10, e1003999. https://doi.org/10.1371/journal.pgen.1003999

Seaver, E.C., Thamm, K., Hill, S.D., 2005. Growth patterns during segmentation in the two polychaete annelids, *Capitella* sp. I and *Hydroides elegans*: comparisons at distinct life history stages. Evolution & Development 7, 312–326. https://doi.org/10.1111/j.1525-142X.2005.05037.x

Shigeno, S., Andrews, P.L.R., Ponte, G., Fiorito, G., 2018. Cephalopod Brains: An Overview of Current Knowledge to Facilitate Comparison With Vertebrates. Front. Physiol. 9. https://doi.org/10.3389/fphys.2018.00952

Stern, C.D., 2006. Neural induction: 10 years on since the "default model." Curr Opin Cell Biol 18, 692–7. https://doi.org/10.1016/j.ceb.2006.09.002

Stern, C.D., 2005. Neural induction: old problem, new findings, yet more questions. Development 132, 2007–21. https://doi.org/132/9/2007 [pii] 10.1242/dev.01794

Struck, T.H., 2011. Direction of evolution within Annelida and the definition of Pleistoannelida. Journal of Zoological Systematics and Evolutionary Research 49, 340–345. https://doi.org/10.1111/j.1439-0469.2011.00640.x

Sur, A., Magie, C.R., Seaver, E.C., Meyer, N.P., 2017. Spatiotemporal regulation of nervous system development in the annelid *Capitella teleta*. EvoDevo 8. https://doi.org/10.1186/s13227-017-0076-8

Sur, A., Renfro, A., Bergmann, P.J., Meyer, N.P., 2020. Investigating cellular and molecular mechanisms of neurogenesis in *Capitella teleta* sheds light on the ancestor of Annelida. BMC Evolutionary Biology 20, 84. https://doi.org/10.1186/s12862-020-01636-1

Tan, S., Huan, P., Liu, B., 2020. Molluscan dorsal-ventral patterning relying on BMP2/4 and Chordin provides insights into spiralian development and bilaterian body plan evolution. bioRxiv 2020.08.11.245670. https://doi.org/10.1101/2020.08.11.245670

Tan, S., Huan, P., Liu, B., 2018. An investigation of oyster TGF-β receptor genes and their potential roles in early molluscan development. Gene 663, 65–71. https://doi.org/10.1016/j.gene.2018.04.035

Treffkorn, S., Mayer, G., 2013. Expression of the decapentaplegic ortholog in embryos of the onychophoran Euperipatoides rowelli. Gene Expression Patterns 13, 384–394. https://doi.org/10.1016/j.gep.2013.07.004

van der Zee, M., Stockhammer, O., Levetzow, C. v., Fonseca, R.N. d., Roth, S., 2006. Sog/Chordin is required for ventral-to-dorsal Dpp/BMP transport and head formation in a short germ insect. Proceedings of the National Academy of Sciences 103, 16307–16312. https://doi.org/10.1073/pnas.0605154103

von Ohlen, T., Doe, C.Q., 2000. Convergence of *dorsal, dpp, and egfr* signaling pathways subdivides the *Drosophila* neuroectoderm into three dorsal-ventral columns. Dev Biol 224, 362–72. https://doi.org/10.1006/dbio.2000.9789 S0012-1606(00)99789-6 [pii]

Weigert, A., Helm, C., Meyer, M., Nickel, B., Arendt, D., Hausdorf, B., Santos, S.R., Halanych, K.M., Purschke, G., Bleidorn, C., Struck, T.H., 2014. Illuminating the base of the annelid tree using transcriptomics. Mol Biol Evol 31, 1391–401. https://doi.org/10.1093/molbev/msu080

Wheeler, S.R., Carrico, M.L., Wilson, B.A., Skeath, J.B., 2005. The Tribolium columnar genes reveal conservation and plasticity in neural precursor patterning along the embryonic dorsal-ventral axis. Dev Biol 279, 491–500. https://doi.org/10.1016/j.ydbio.2004.12.031

Wilson, M.J., Kenny, N.J., Dearden, P.K., 2014. Components of the dorsal-ventral pathway also contribute to anterior-posterior patterning in honeybee embryos (*Apis mellifera*). Evodevo 5, 11. https://doi.org/10.1186/2041-9139-5-11

Wilson, S.I., Edlund, T., 2001. Neural induction: toward a unifying mechanism. Nat Neurosci 4 Suppl, 1161–8. https://doi.org/10.1038/nn747 nn747 [pii]

Xiao, Z., Brownawell, A.M., Macara, I.G., Lodish, H.F., 2003. A Novel Nuclear Export Signal in Smad1 Is Essential for Its Signaling Activity. J. Biol. Chem. 278, 34245–34252. https://doi.org/10.1074/jbc.M301596200

Yamaguchi, E., Seaver, E.C., 2013. The importance of larval eyes in the polychaete *Capitella teleta*: effects of larval eye deletion on formation of the adult eye. Invertebrate Biology 132, 352–367. https://doi.org/10.1111/ivb.12034

Zhao, D., Chen, S., Liu, X., 2019. Lateral neural borders as precursors of peripheral nervous systems: A comparative view across bilaterians. Development, Growth & Differentiation 61, 58–72. https://doi.org/10.1111/dgd.12585

Tables

Table 1. Published effects of early BMP exposure or BMP knockdown in spiralians. Wildtype: Wt; N/A: not applicable.

Phylum	Species	Reference	Exogenous BMP4 protein phenotype			
			Overall episphere effect	eyes		brain
				1q–3q	4q	1q–3q
Annelida	*Ca. teleta*	this study	major	loss larval; gain juvenile	gain larval and juvenile	radialized
Mollusca	*Cre. fornicata*	Lyons et al 2020	major - 1q pinches off	loss	wt	radialized
	Tr. obsoleta	Lambert et al 2016	major	gain	N/A	gain
	L. goshimai	Tan et al 2020	N/A	loss (zygote- gastrulation)	gain	N/A
			BMP knockdown phenotype			
			method	**brain**	**organizer effect**	**foregut**
Annelida	*Ca. teleta*	Lanza and Seaver 2018, 2020a	dorsomorphin, SMAD1/5/8 morpholino	symmetrical	not a phenocopy	loss
	H. sp (Austin)	Kuo and Weisblat, 2011	BMP5-8 morpholino	N/A	ventralization of segmental ectoderm	N/A
	Ch. pergamentaceus	Lanza and Seaver 2020b	dorsomorphin, DMH1	wt	wt	wt
Mollusca	*Cre. fornicata*	Lyons et al 2020	DMH1	expansion	not a phenocopy	extra
	Tr. obsoleta	Lambert et al 2016	BMP2-4 morpholino	N/A	phenocopy	loss
	L. goshimai	Tan et al 2020	Bmp2-4 morpholino	Wt	radialization	N/A
			Chordin morpholino	expansion	radialization	
	Cra. gigas	Tan et al 2018	dorsomorphin	N/A	ventralization of gene expression patterns	N/A
Brachiopoda	*N. anomala* and *Te. transversa*	Martín-Durán et al 2016	DMH1	expansion of markers for anterior ectoderm and mesoderm; ventral ectoderm	N/A	N/A

Figure captions

Figure 1. List of exogenous BMP4 treatments performed. Stage timings are approximate. Blue dashed line: Animals raised in pen/strep ASW. Blue tissue in stages 4-6: neural tissue.

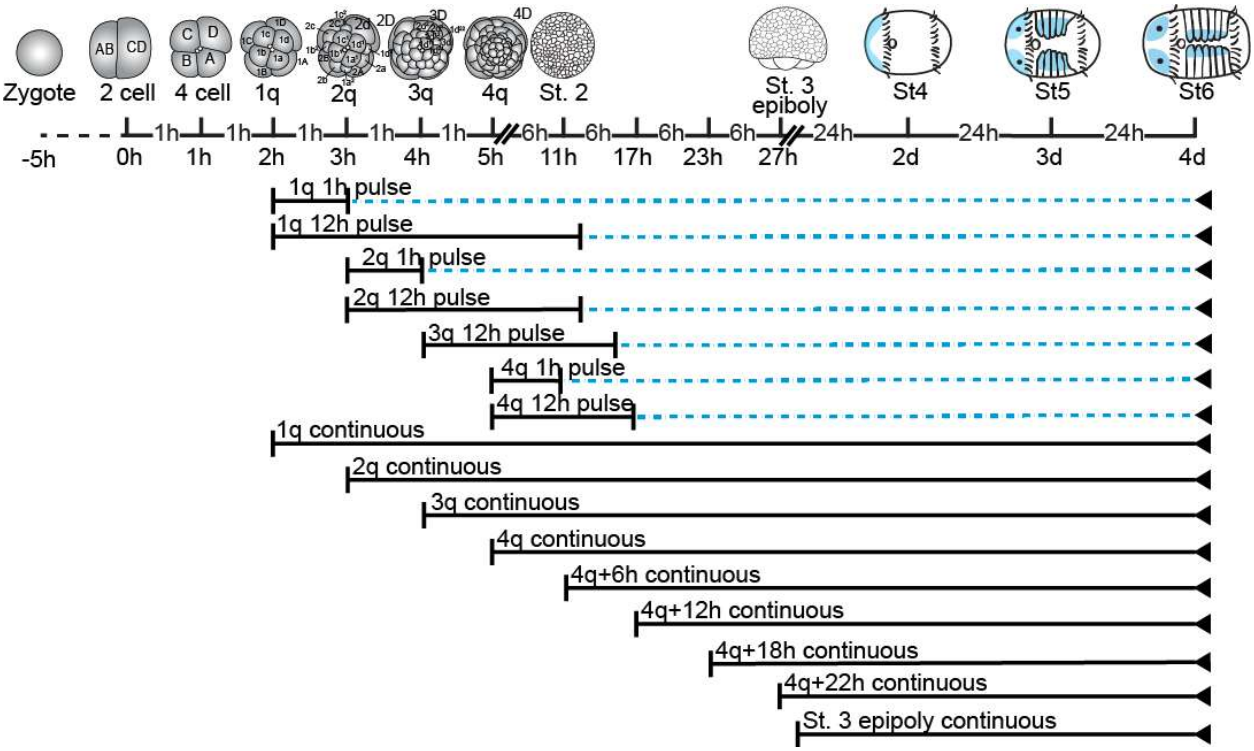

Figure 2. Western blot of pSMAD1/5/8 on 2q animals with either mock for 6 h or BMP for 10min, 1 h, 3 h, or 6 h (n = 40 per lane). *, presumed pSMAD1/5/8; arrow, unknown band, see text.

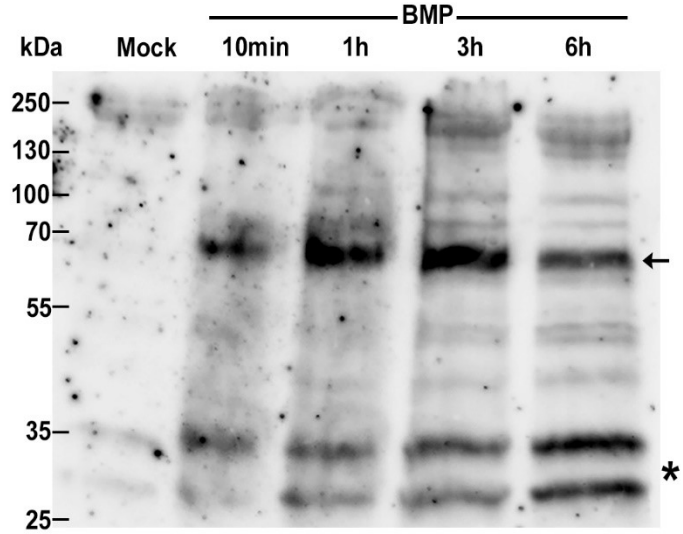

Figure 3. SMAD Alignments of *C. teleta* A) SMAD1/5/8 showing the loss of the conserved start codon (~18aa), the next start codon at 225 aa. B) SMAD2/3 and SMAD1/5/8 alignments showing the conserved C-terminus where the pSMAD1/5/8 antibody 41D10 and the pSMAD2/3 antibody D27F4 bind. Species are as follows: Ct-*Capitella teleta*, Hro – *Helobdella robusta*, Crg – *Crassostrea gigas*, Hu – human, and the spider Stm - *Stegodyphus mimosarum*. Protein domains: MH1, MAD homology 1; MH2, MAD homology 2; NES, nuclear export signal; NLS, nuclear localization signal.

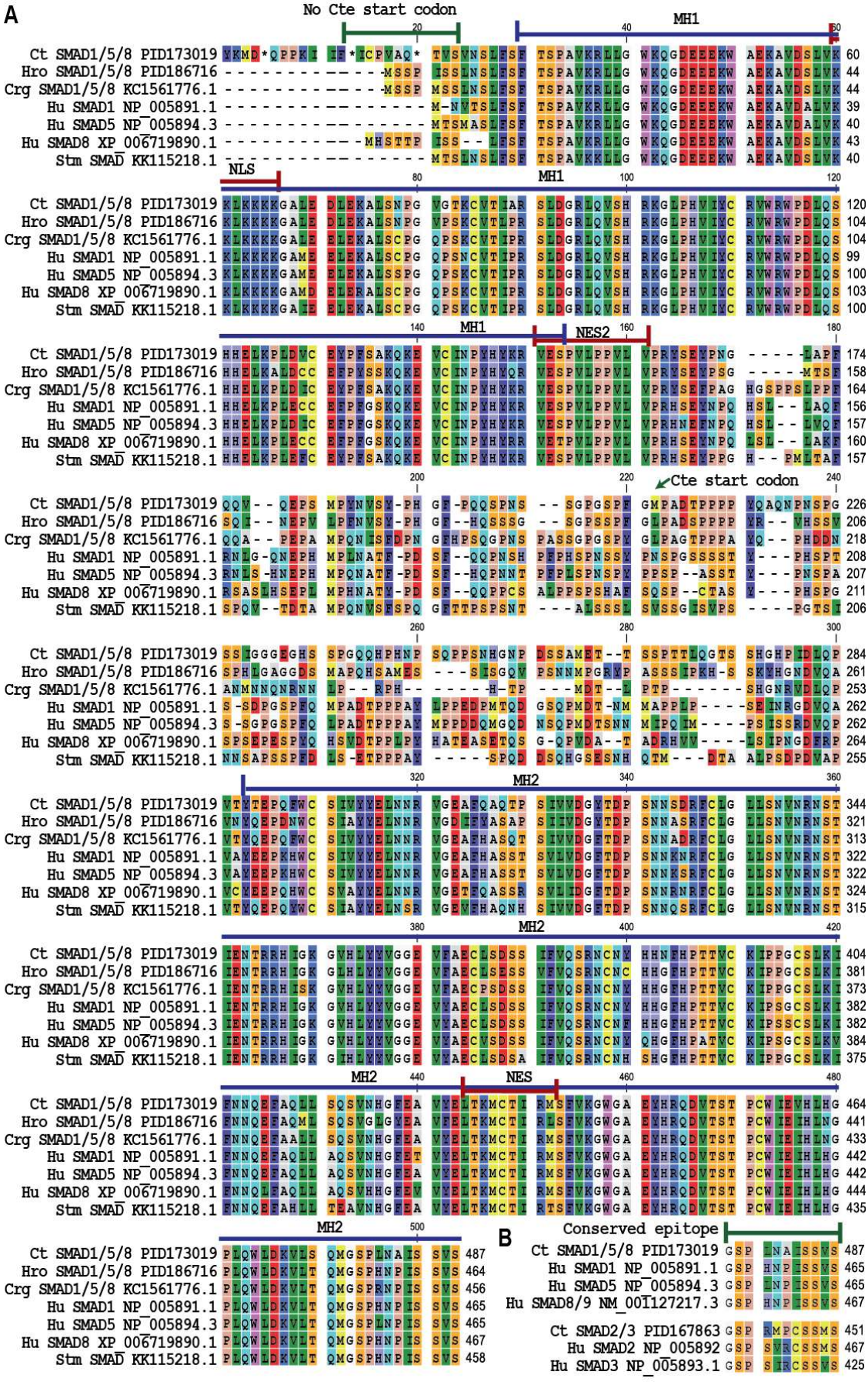

Figure 4. Left lateral z-stacked DIC images showing D-V axis formation in A) Mock, B) 1q pulse, and C) 4q pulse animals. brain, B (blue); foregut, fg (yellow); prototroch, pt; telotroch, telotroch; VNC (green), A, anterior, D, dorsal.

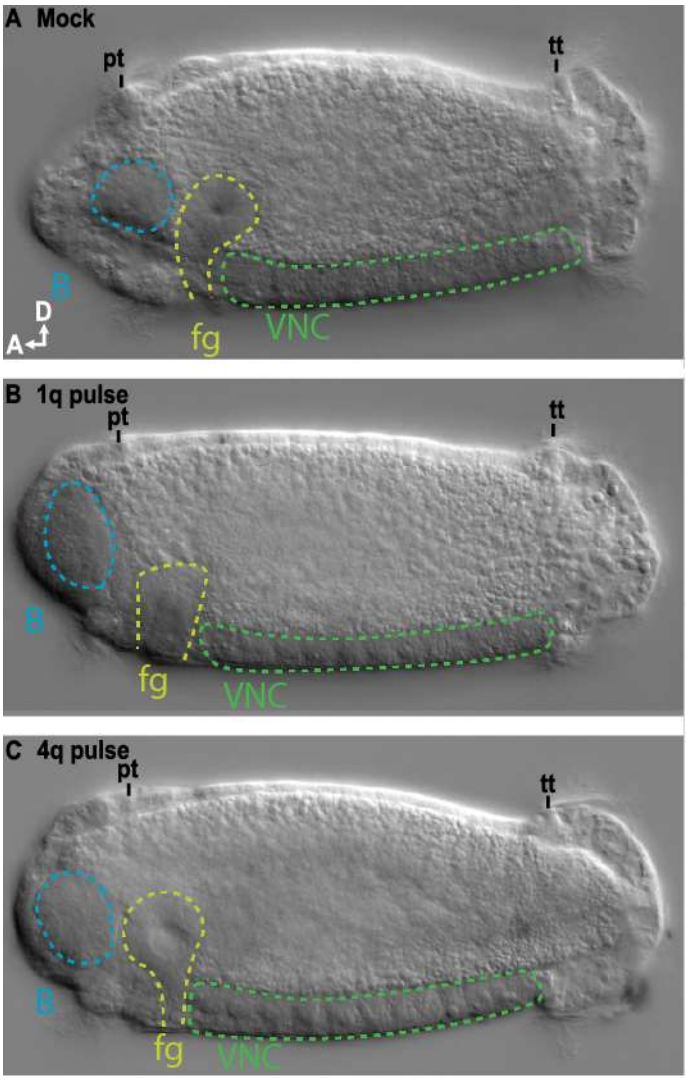

Figure 5. *Ct-chrdl* expression. (A-B) Dorsal z-stack of *Ct-chrdl* mRNA expression in (A) Mock and (B) 3q cont BMP treated animals. C) Boxplot showing the significant effect of BMP treatment on the width of Ct-chrdl expression, letters indicate significance groups. A, anterior, R, right side, scale bar = 50 µm.

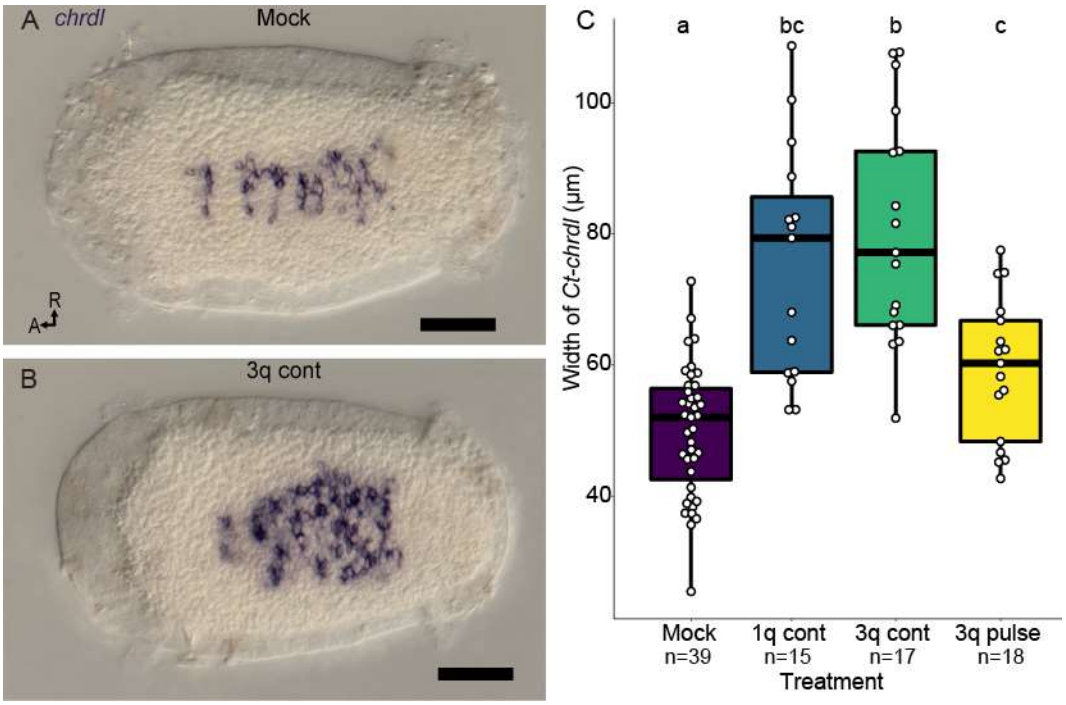

Figure 6. *Ct-Elav1* expression in BMP-treated animals. (A-D) Mock (n = 37), dashed lines in (C) represent focal depths of (A) and (B). (E-H) 1q pulse (n = 36). (I-L) 4q pulse (n = 36). (M-P) 1q cont (n = 45) showing collapse of some hemiganglia expressing Elav1. Scale bar = 50 μm; br: brain, VNC: ventral nerve cord.

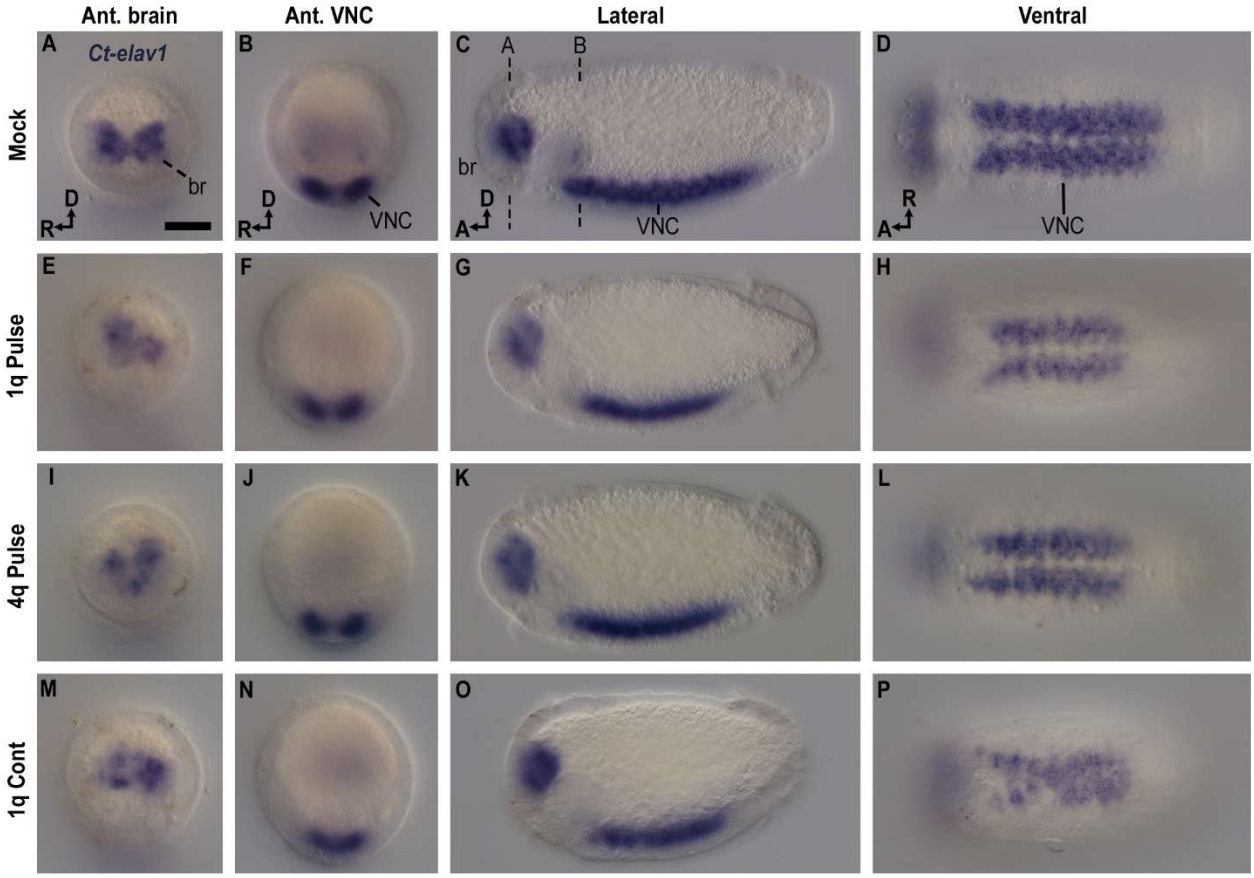

Figure 7. Ventral z-stack of the serotonergic nerves (white), and anti-acetylated-Tubulin staining (red) in the VNC with a nuclear stain (blue). Only minor disorganization was seen in 1q pulse (B), 4q pulse (C), or st 3 cont (D) animals compared to mock (A). A, anterior, L, left side.

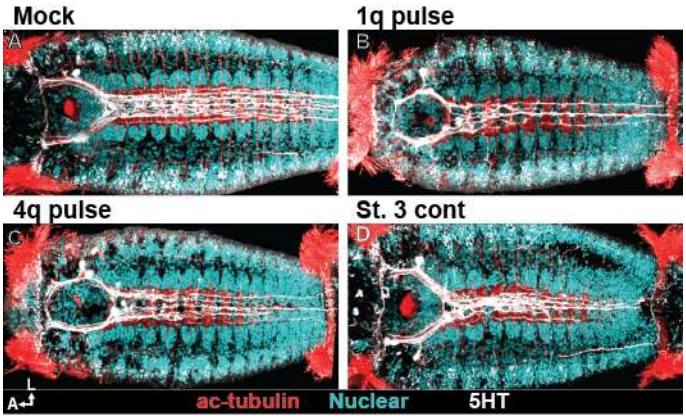

Figure 8. Trunk neural phenotype in cont BMP-treated (Z-stack). (A,D,G,J,M) A mock animal showing wild-type phenotype. (B,E,H,K,N) A 4q+12h continuous animal showing a mild VNC collapse phenotype. (C,F,I,L,O) A 4q+12h continuous animal showing a severe VNC collapse. (A-C) Serotonin, (D-F) acetylated-Tubulin in the VNC. (G-I) Hoechst nuclear stain. (J-L) Merge: Serotonin: magenta, ac-Tubulin: white, nuclear: cyan. (M-O) ac-Tubulin showing neurotroch cilia. A, anterior, L, left side, scale bar = 50 µm (P) Boxplot showing the significant effect of treatment on proportion of segments with collapsed hemiganglia, letters indicate significance groups.

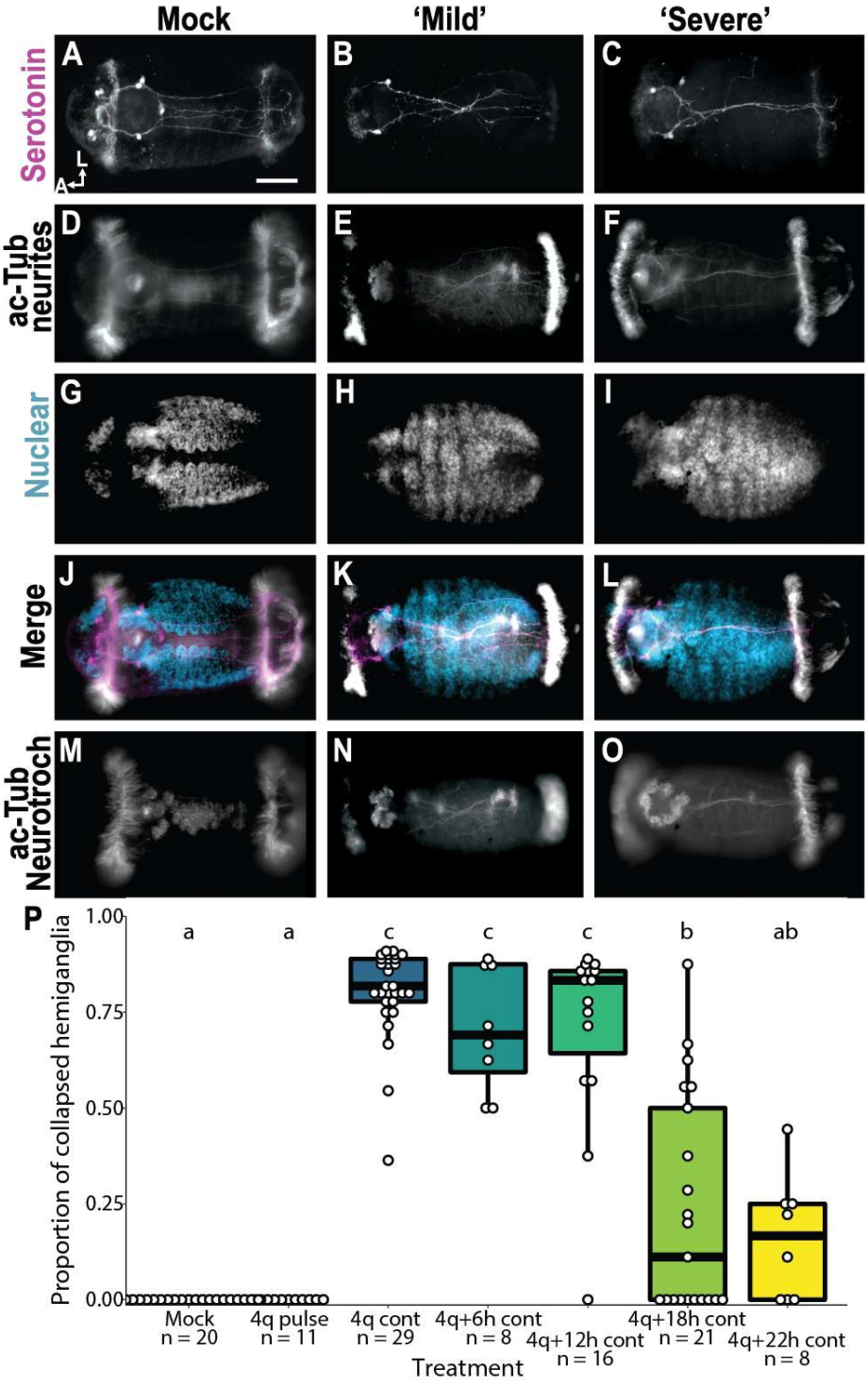

Figure 9. Trunk main connectives collapse (Z-stack). (A,D) Synapsin, (B,E) FMRF-like immunoreactivity, (C,F) Pax. (A-C) Mock animals. (D-E) 4q cont animals. E) st. 2 cont animal. Animals in A,D are smaller than B,C,E, F. A, anterior, L, left side, scale bar = 50 µm

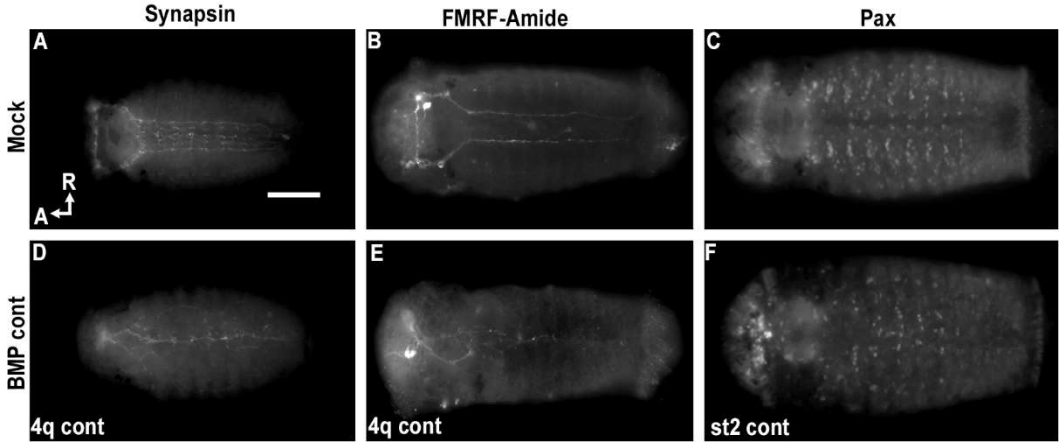

Figure 10. Larval eye pigment cells. A-D Most common eye phenotypes, anterior view. A) 0 eyes, B) 2 wild-type eyes, C) 3 eyes centered, D) 3 eyes stacked. R, right side, D, dorsal. E. Proportion of animals with each eye phenotype in each BMP treatment. Letters indicate significance groups.

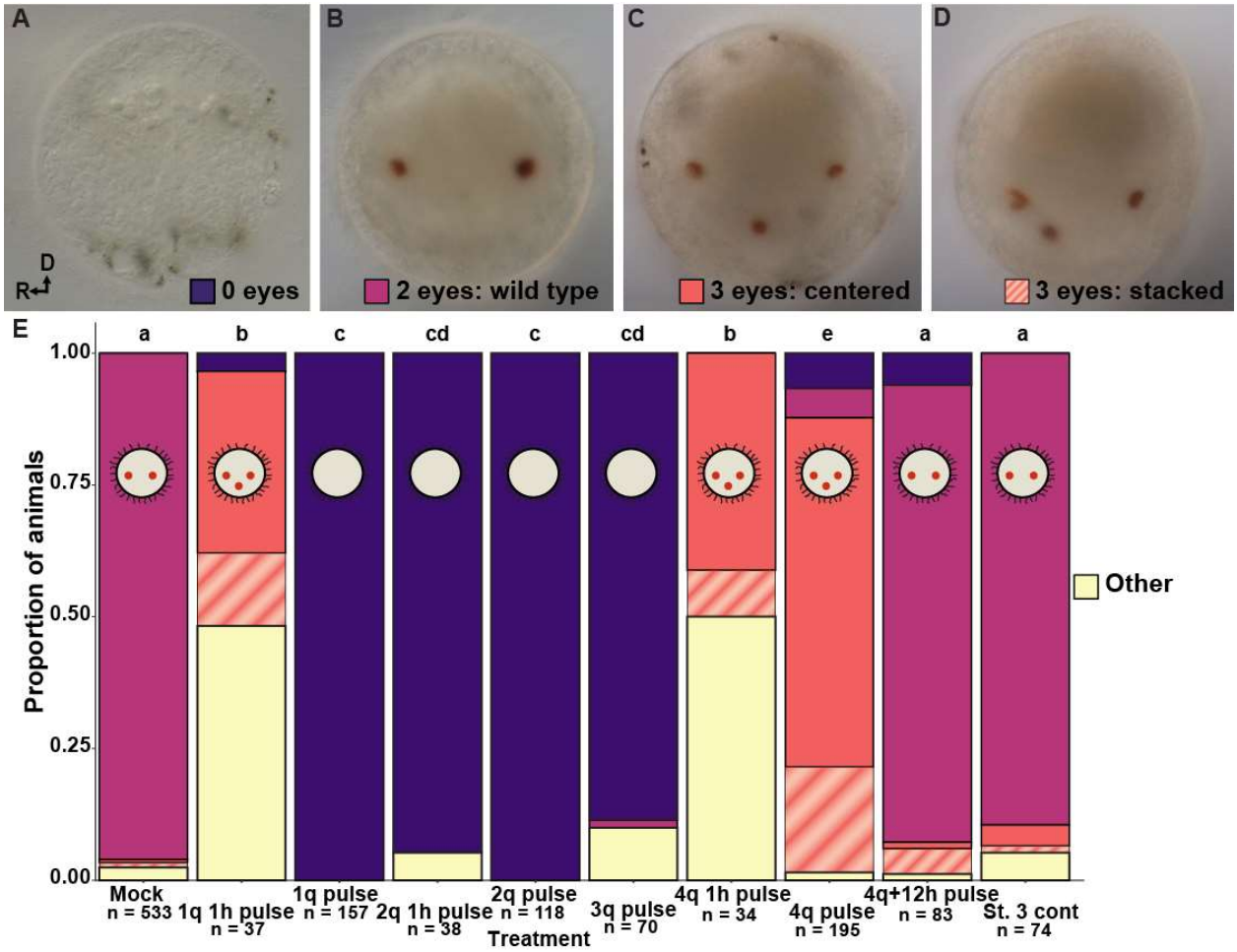

Figure 11. The effect of BMP treatment on larval and juveniles sensory cells (SCs). A-E) Each larval SCs was associated with an eye pigment cell. F-J) BMP increased the number of juvenile eye SCs. A) Proportion of animals with each larval SC phenotype in each BMP treatment. Letters indicate significance groups. B-E, G-L) Anterior z-stack of 22c10 showing (B-D) larval SCs (yellow, arrows), nuclei (teal), and muscles (magenta). E) Image of single larval SC. F) Proportion of animals with each number of juvenile SCs in each BMP treatment. G-L) juvenile SCs (arrowheads). B,G) Mock, C,H) 1q pulse, and E,I) 4q pulse animals. R, right side, D, dorsal, scale bars = 50 μm.

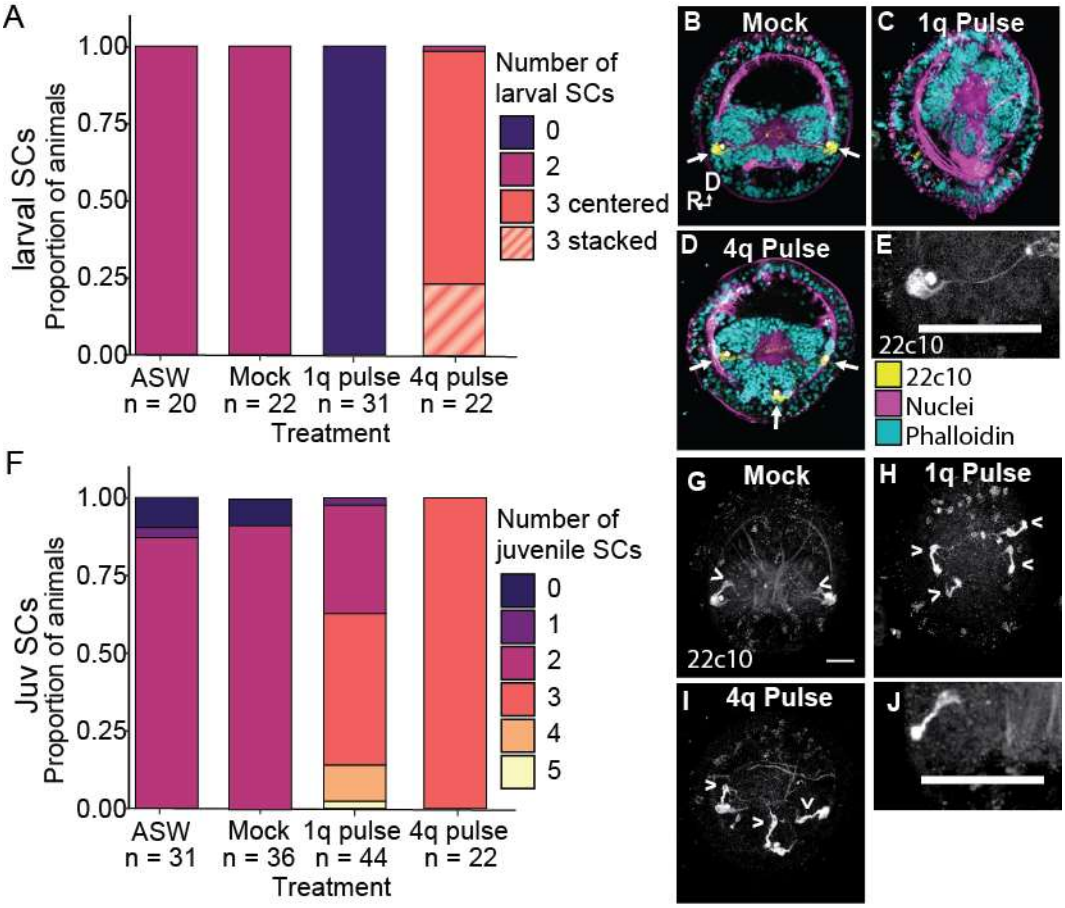

Figure 12. Localization of 5HT in the episphere. A-D) ASW (A) and Mock (B-D) treatment animals had a symmetric bimodal distribution of 5HT cells showing a left and right brain lobe. E-I) 1q (E), 2q (F-H), and 3q (I) pulse BMP treatment animals showed a uniform distribution of 5HT cells, showing a radialized brain. J-L) 4q pulse animals showed a bimodal ventral distribution of 5HT, showing a ventralization of the brain. AB, EF, IJ) Percent of animals with 5HT cells in each region of the episphere. C,F,I) stacked immunostaining of 5HT in 3 treatments representative of the 3 brain states. D,H,I) stacked immunostaining of 5HT (magenta), ac-tubulin (white), and nuclei (cyan).White arrows: Mean vectors(s) of 5HT localization model, scale bars: 50 μm.

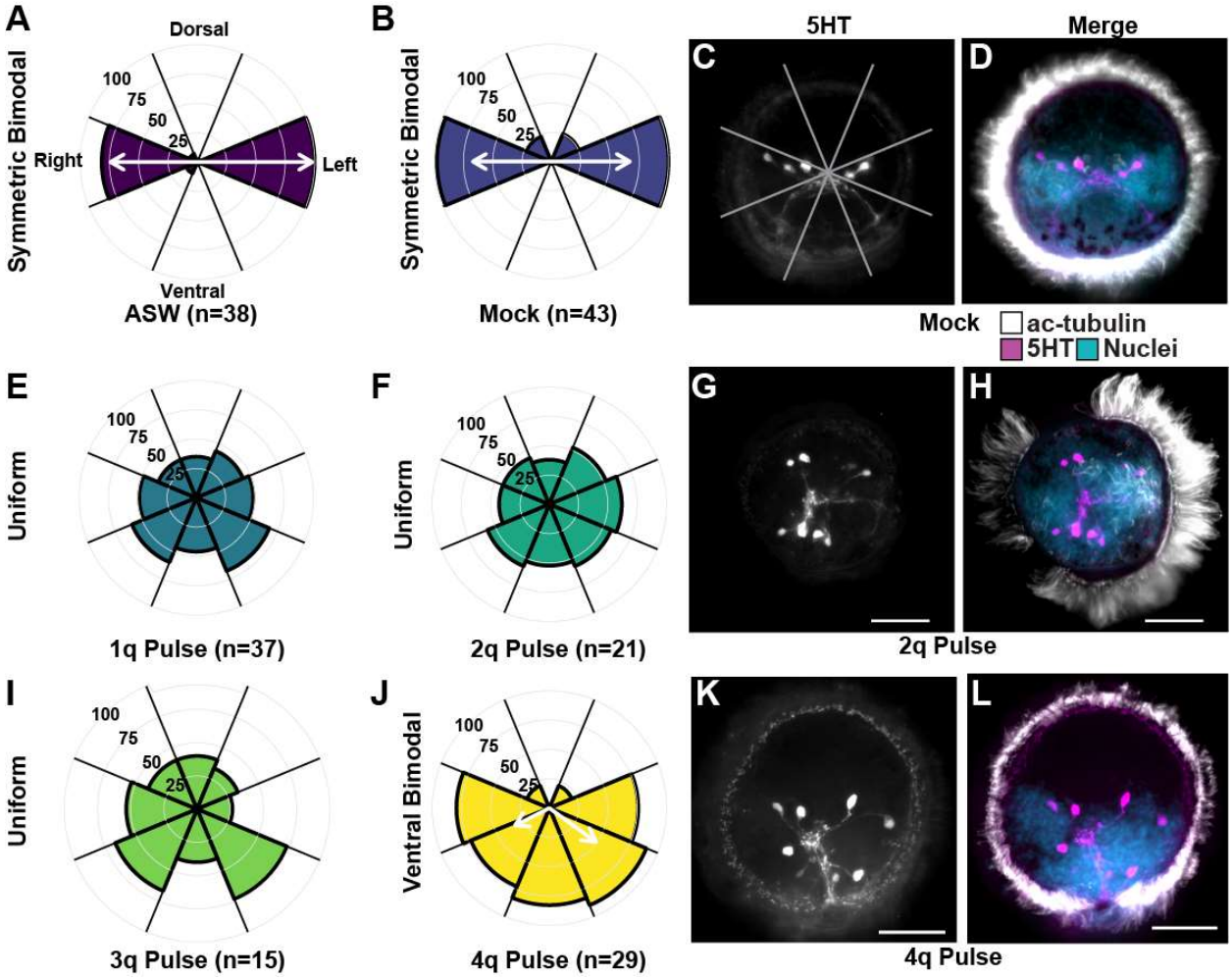

Figure 13. DiI localization and fate map of the eyes and brain of animals treated with BMP with a 4q pulse (Z-stack). A-B) 1b injected, showing contributions to A) the central brain lobe and eye or B) both the central and right eyes. C-D) 1a injected, showing contributions to C) The left eye and brain lobe or D) both the central and left eyes. E) Contribution of 1q micromeres to the episphere in wildtype animals. F) Predicted contribution 1q micromeres including the contribution of 1b to the third ectopic eye in BMP treated 3-eyed animals. Numbers in the top left indicate the number of animals with the displayed phenotype / total. Arrowheads, eye location; pink closed arrowhead; eye with DiI; white open arrowhead, eye without DiI; cyan, nuclei; yellow, phalloidin; magenta, DiI scale bar = 50 μm.

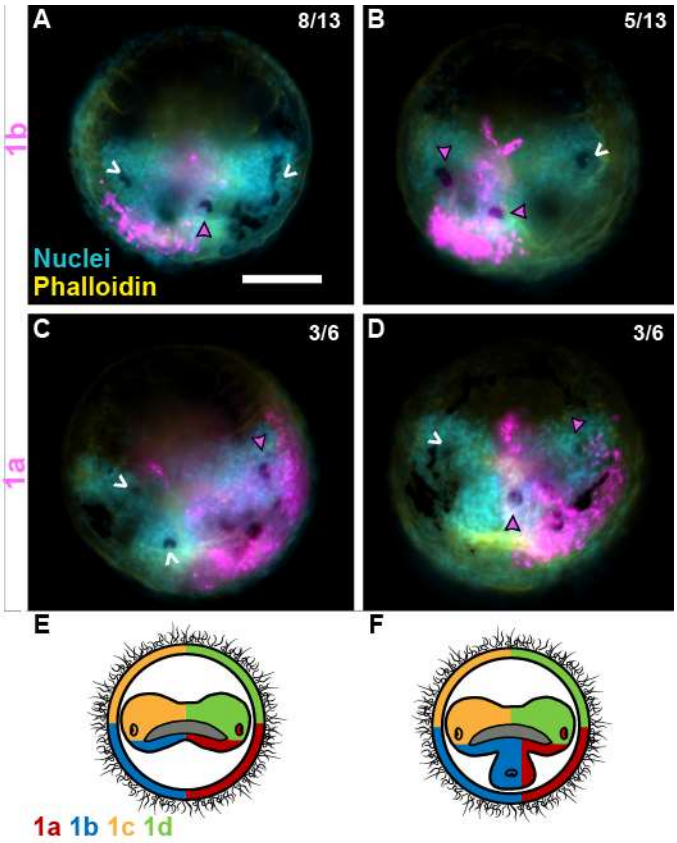

Figure 14. The effect of BMP treatment on foregut morphology. A) Bilobed foreguts in mock and ASW control animals. B) 1q, 2q, and 3q pulse animals had small round foreguts (100%). C) Foreguts of 4q pulse animals were trilobed (100%). (D-E) Total foregut area was significantly smaller in animals subjected to 1q, 2q, 3q, and 4q BMP pulse than the controls. Animals in E were fixed at a later stage than animals in D and could not be compared due to significant size difference in mock animals. brain, br; foregut, yellow dashed line; scale bar: 50 μm

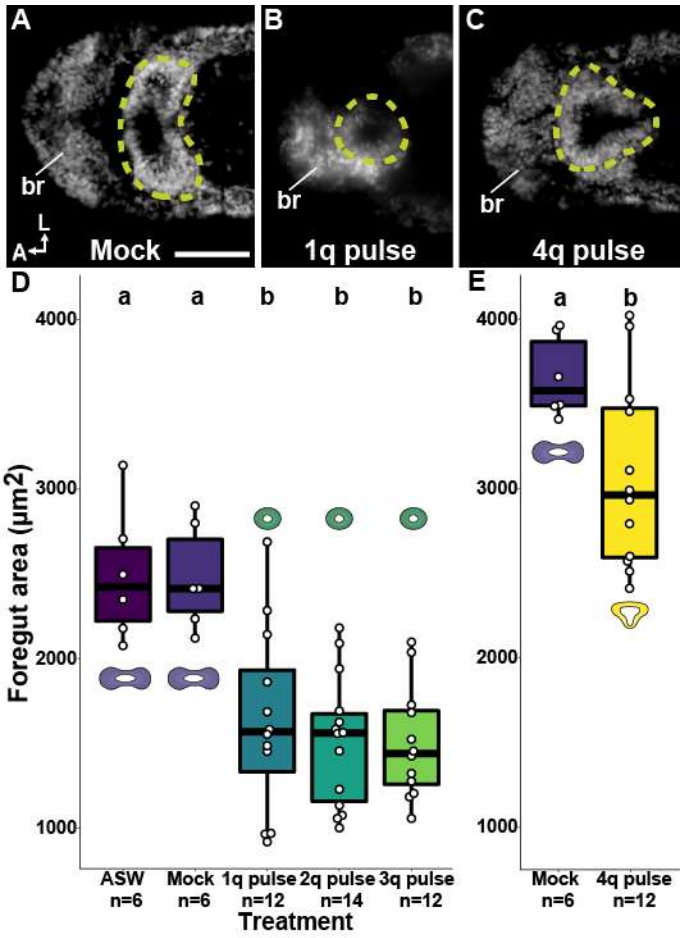

Figure 15. Overview of our BMP treatment results and hypothesized fate switching time windows in *C. teleta*.